Naval Research Laboratory
Washington, DC 20375-5320

NRL/5310/MR—2022/3

Final Report on Modal Beamformers using Passive Butler Matrices

RASHMI MITAL

WILLIAM R. PICKLES

Antenna Section
Radar Division

October 12, 2022

REPORT DOCUMENTATION PAGE

Form Approved
OMB No. 0704-0188

1. REPORT DATE *(DD-MM-YYYY)*	**2. REPORT TYPE**	**3. DATES COVERED** *(From - To)*
12-10-2022	NRL Memorandum Report	Dec 20 – Oct 21

4. TITLE AND SUBTITLE

Final Report on Modal Beamformer Using Passive Butler Matrices

5a. CONTRACT NUMBER

5b. GRANT NUMBER

5c. PROGRAM ELEMENT NUMBER
62271N

6. AUTHOR(S)

Rashmi Mital (PA) and William R. Pickles

5d. PROJECT NUMBER

5e. TASK NUMBER
EW-271-001

5f. WORK UNIT NUMBER
6B48

7. PERFORMING ORGANIZATION NAME(S) AND ADDRESS(ES)

Naval Research Laboratory
4555 Overlook Avenue, SW
Washington, DC 20375-5320

8. PERFORMING ORGANIZATION REPORT NUMBER

NRL/5317/MR--2022/3

9. SPONSORING / MONITORING AGENCY NAME(S) AND ADDRESS(ES)

Office of Naval Research
One Liberty Center
875 N. Randolph Street, Suite 1425
Arlington, VA 22203-1995

10. SPONSOR / MONITOR'S ACRONYM(S)

ONR

11. SPONSOR / MONITOR'S REPORT NUMBER(S)

12. DISTRIBUTION / AVAILABILITY STATEMENT

DISTRIBUTION STATEMENT A: Approved for public release; distribution is unlimited.

13. SUPPLEMENTARY NOTES

14. ABSTRACT

Antennas that have elements placed in a circular fashion require complex beamforming strategies as each element has a different pointing direction and thus the overall radiation pattern cannot be simplified as for planar arrays. However by transforming the circular elements into phase modes using a passive Butler matrix we can create elements that now behave similar to elements in a planar array. In this report we present the final hardware designs for the 4 X 4 and 8 X 8 Butler matrices. We also demonstrate the formation of phase modes from passive beamformers and show the formation of directional beams as well as beams with nulls.

15. SUBJECT TERMS

16. SECURITY CLASSIFICATION OF:			**17. LIMITATION OF ABSTRACT**	**18. NUMBER OF PAGES**	**19a. NAME OF RESPONSIBLE PERSON**
a. REPORT	**b. ABSTRACT**	**c. THIS PAGE**			Rashmi Mital
U	U	U	U	30	**19b. TELEPHONE NUMBER** *(include area code)* (202) 767-2584

This page intentionally left blank.

CONTENTS

Table of Figures

EXECUTIVE SUMMARY

Cylindrical and circular arrays have the unique ability to offer a full 360° field-of-view (FOV) using either omnidirectional or directional beams without the need to handoff between multiple faces as with multi-face planar arrays. However, conventional beamforming techniques require complex optimization methods to set the amplitude and phase weights at each element of the circular/cylindrical arrays. In this research project, we investigated a methodology to help simplify the beamforming for these unique arrays using modal beamformers. A modal beamformer has two functional blocks: a Fast Fourier Transform (FFT) block and an equalizer block. The FFT block transforms the circular array radiation patterns into phase modes while the equalizer calibrates patterns to remove any frequency differences. In this report, we present the final models, designs and hardware for each of the functional blocks as well as the generation of phase modes from radiation patterns of circular elements.

As a part of this 6.2 effort, we completed theoretical designs of the FFT block for N-ports using passive Butler matrices. Wideband phase shifter designs, optimized to operate from 2GHz to 6GHz, were used as a common component in these passive, analog designs. Designs for the 4×4 and 8×8 Butler matrices were completed, and built. The measurements for the 4×4 Butler matrix are presented in this report. Finally, we discuss how using this simple modal beamformer transforms the circular array elements into phase modes that are then weighted to form beams. Figure E-1 shows the transformation of a circular array to a simpler linear array.

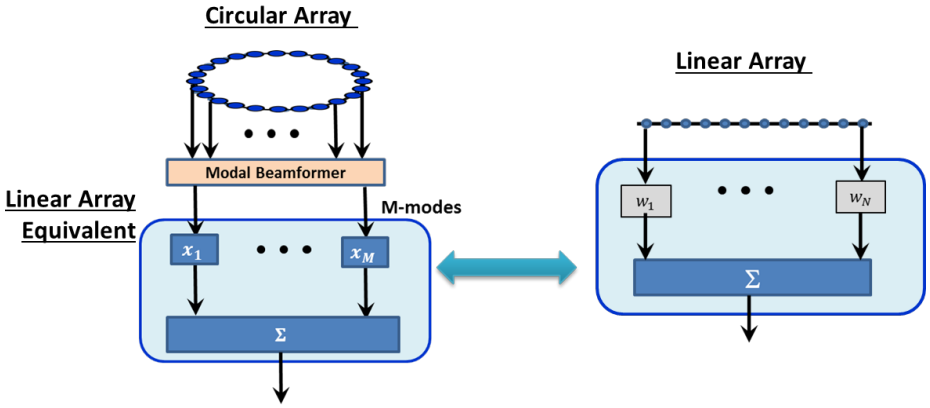

Figure. E-1 — Transforming a circular array elements to emulate the elements of a linear array

1. INTRODUCTION

The future objective of the Navy is to reduce the number of topside masts and the number of single-function antennas to help reduce platform signature and acquisition cost. While the desired number of radiating apertures are decreasing, the required number of wideband functions, such as Radar, Signal Intelligence (SIGINT) and Electronic Warfare (EW), is increasing. New Navy efforts such as Project Overmatch and Scepter require a 360° field of view (FOV) over wide bandwidths. These requirements conventionally use a multi-face planar array that need to be oversized to compensate for scan loss due to beam steering off broadside.

Cylindrical phased arrays can satisfy many of the stringent requirements placed on multifunction apertures because of their ability to offer a full 360° FOV using either omnidirectional or directional beams without the need for handoff between the various faces. Furthermore, unlike planar or linear arrays, cylindrical arrays do not suffer from scan loss as the beam scans in the azimuthal direction. However, traditional beamforming techniques are complicated for circular and cylindrical arrays. This is because every element has a unique pointing direction, making beamforming dependent on scan angle and frequency [1]. Phase mode transformation techniques are most effective when implementing beamforming for circular or cylindrical arrays [2].

Over the last few years, we have had an internal 6.2 [WU6B48] program, which focusses on utilizing Butler matrices to transform element-level signals of a circular phased array into phase modes. We have published in detail, the methodology of this technique in earlier reports [1, 3].

As an overview, phase modes have unit amplitude and phase that cycles between -180° and +180°; with the number of cycles depending on the mode number – see Figure 1-1. This figure only shows the phase variation of phase modes. Each phase mode has a radiation pattern of $e^{jM\phi}$ where M is the phase mode and ϕ is the radiation angle. Figure 1-1 shows the phases variation of the first three modes. For example, Mode 1 cycles between -180° and +180° once while mode 2 cycles twice and mode N cycles N times. To form a directional beam, these phase modes are weighted, phased and summed [2]. Thus, phase modes function as elements in an equivalent linear array.

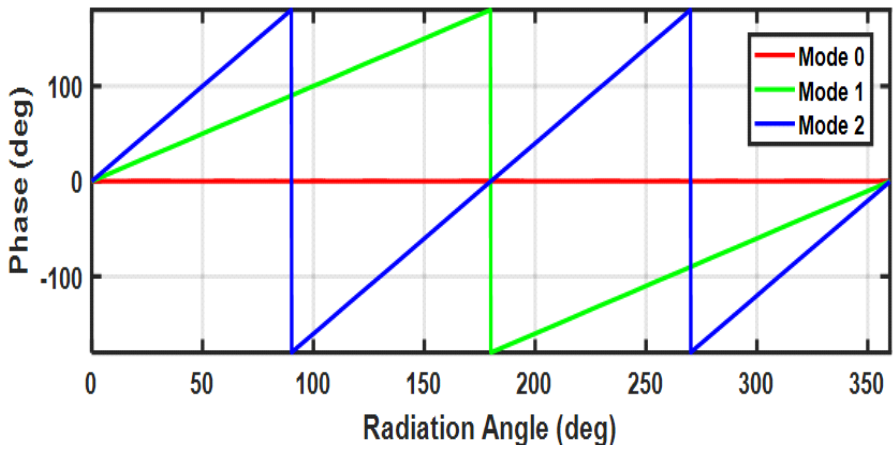

Figure 1-1 : Example of phase variation of phase modes vs. radiation angle. Mode 0 has no phase change while Mode 1 cycles between -180° and +180° once and Mode 2 cycles twice.

In earlier reports, we discussed how Butler matrices are used to design an analog modal beamformer due to their unique ability to provide a "flat" phase shift across the band of operation. We presented simulations

Manuscript approved October 10, 2022.

and designs of these Butler matrices in [1, 3]. In this report, we present simulated and measured results for a 4 × 4 Butler matrix, and simulated data for an 8 × 8 Butler matrix. We show how to generate phase modes and leverage them for beamforming.

2. MEASURED DATA FROM A 4 X 4 BUTLER MATRIX

In the last year, we designed and built a 4 X 4 Butler matrix on a Rodgers 4035. This circuit card design of the Butler matrix uses surface mounted, 180-deg hybrid parts purchased from Werlatone[1], and in-house designed 90-deg phase Shiffman phase shifters [4] and cross-over networks. Figure 2-1 shows the layout of the completed circuit card in AutoCAD®.

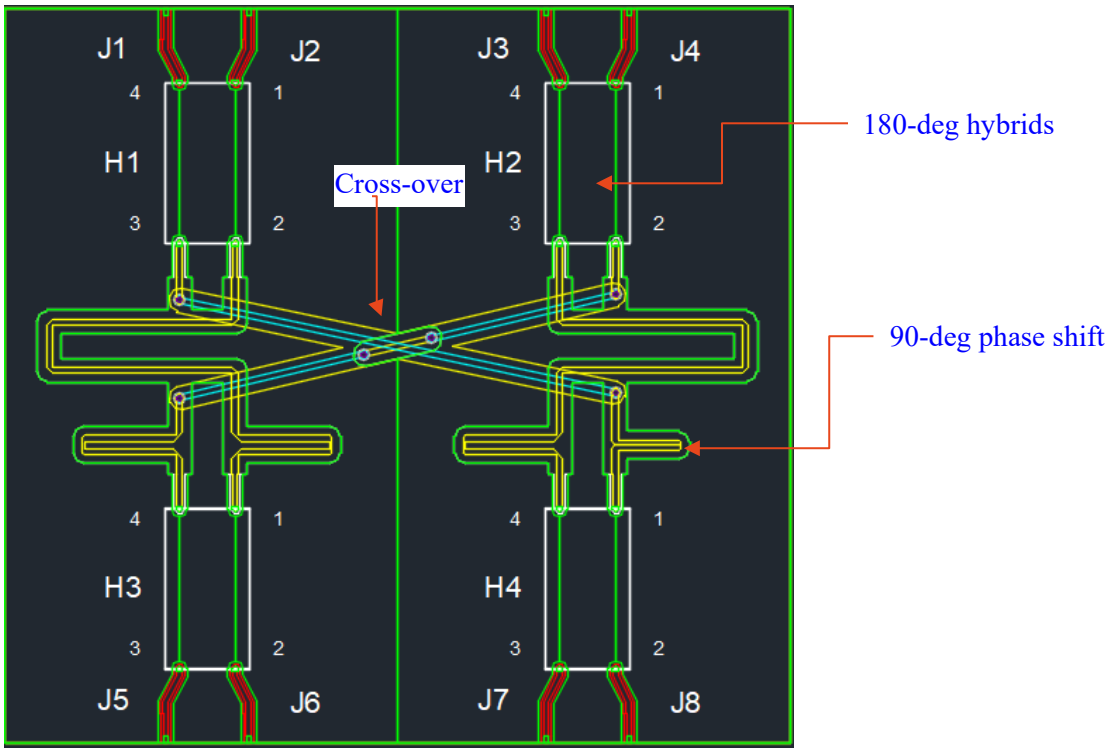

Figure 2-1: Circuit card art showing the 4 X 4 Butler matrix layout.

Figure 2-2 shows the actual circuit card. This is a two-layer card in which the crossover is directed from the top layer to the bottom layer using vias. In addition, the card has vias along the microstrip lines to help dissipate any propagating modes generated in the channels. Reference [3] details the design of this circuit card including the optimization process.

Metal plates covered the top and bottom of this circuit cards. Grooves were cut into the metal plates where the microstrip lines and hybrids are located. In addition, the metal plates have screw holes. These had two uses, one to join the three pieces together and the second to break up any leaky modes that may start propagating in the microstrip channels. These metal plates, top and bottom, are shown in Figure 2-3.

[1] https://www.werlatone.com/180-hybrids/h10126/

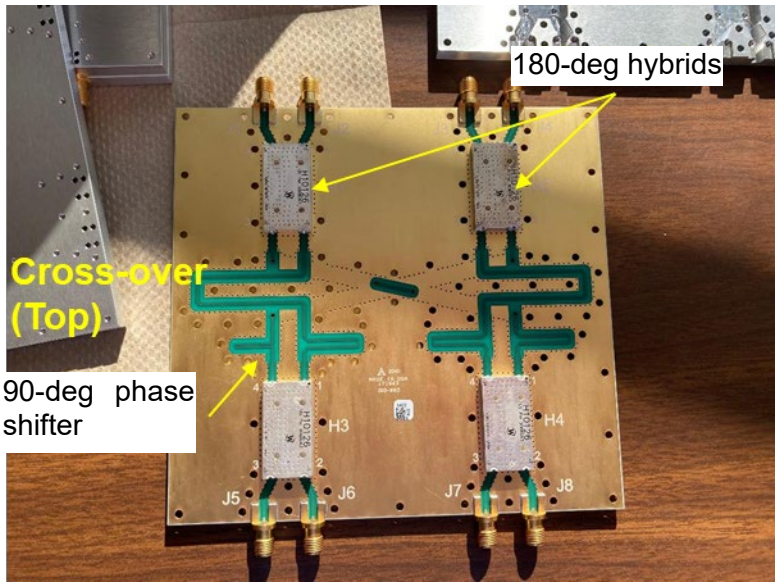

(a) Top View

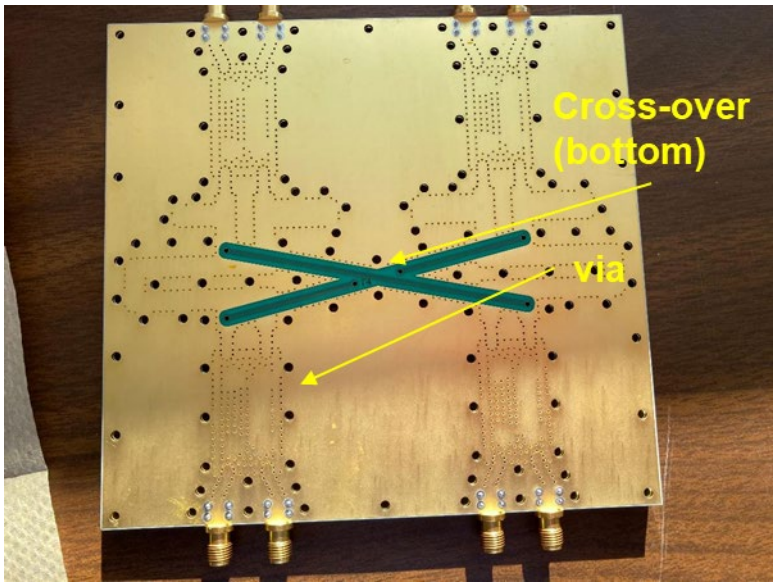

(b) Bottom View

Figure 2-2: (a) Top and (b) bottom view of a 4 X 4 Butler matrix circuit card. This is a two-layer board with vias for the crossover as well as to improve isolation performance. We designed the 90-deg phase shifter using microstrip lines. The details of this design are in [3].

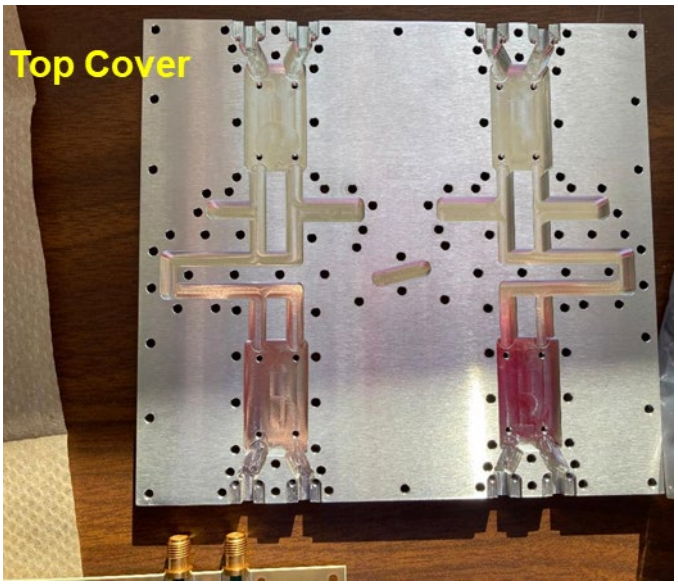

(a) Top metal cover

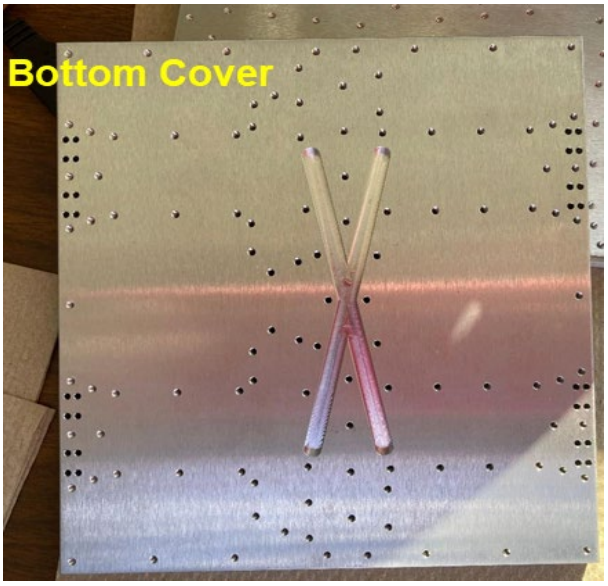

(b) Bottom metal cover

Figure 2-3: (a) Top and (b) bottom metal covers for the 4 X 4 Butler matrix circuit card. The grooves in the metal covers are where the 180-deg hybrid and microstrip lines are. Screws were put in around these lines to both break up leaking modes and to hold the circuit card together.

Once assembled, we measured the 4 X 4 Butler matrix for a full set of S-parameters over a frequency range of 2GHz to 6GHz. To verify performance, we initially modeled the 4 X 4 Butler matrix in Keysight's Genesys® software. This software takes in S-parameters, whether from models or measurements, and cascades them to build an overall RF model. Figure 2-4 shows an example of this layout.

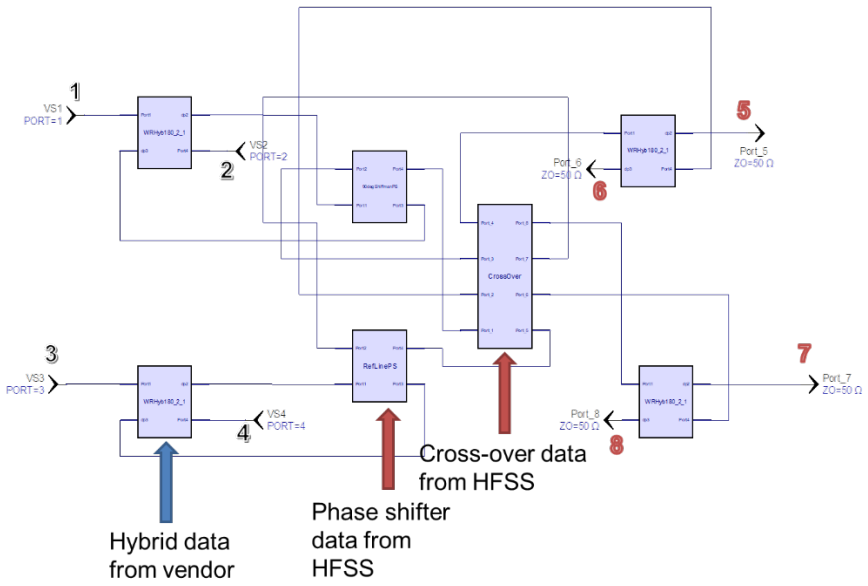

Figure 2-4: An example of a wideband 4 X 4 Butler matrix as modeled in Genesys. The data for the different components (i.e. 180-deg hybrid, phase shifter, cross-over) are obtained either from measurements or models.

We built and measured two boards, referred to in this document as Board A and Board B, for the 4 X 4 Butler matrix. Figure 2-5 and Figure 2-6 show a subset of the measured data. In the figures, the insertion loss and relative phase for the various paths are shown. The input paths have labels of 1 to 4 and the output paths have labels ranging from 5 to 8. Figure 2-5 shows the measurements for Board A. Note the following from these measurements:

- The path loss for S_{51} is extremely high -- this was a bad path. The higher loss may be due to channel leakage or a shorted path.
- Because of the non-working S_{51} path, ripples are observed in all of the phase paths starting from Port 1. Since Board B performed well for this same path, the high insertion loss was attributed to a bad circuit path in Board A.
- For the remaining paths in Board A, the phase remains within $\pm 10^{o}$ of design. In all the figures, the dashed lines are simulation while the solid lines are from measured data.

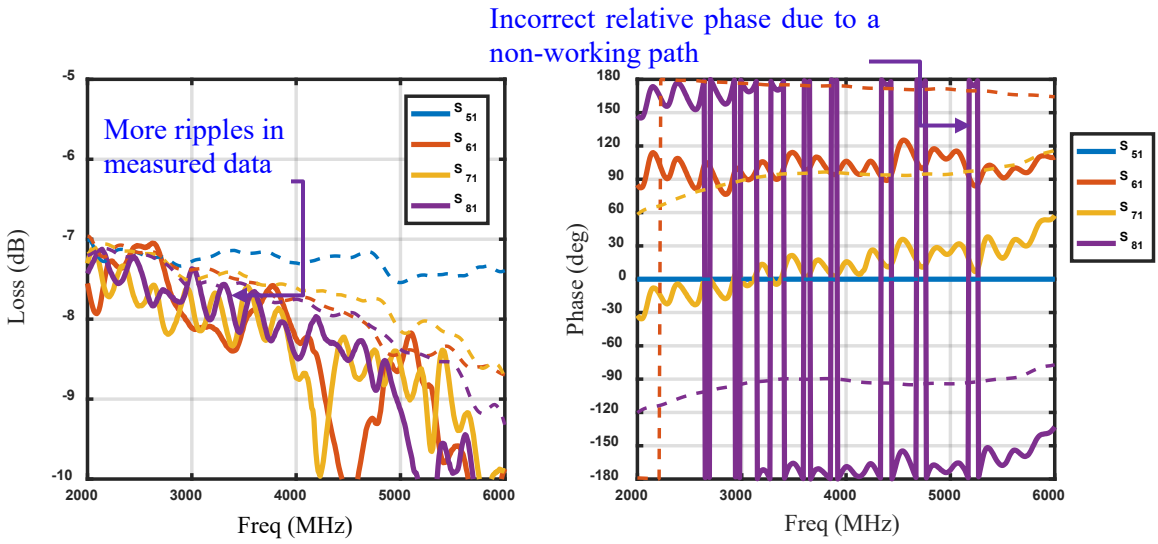

(a) Insertion loss and relative phase between input port 1 and output ports 5 – 8.

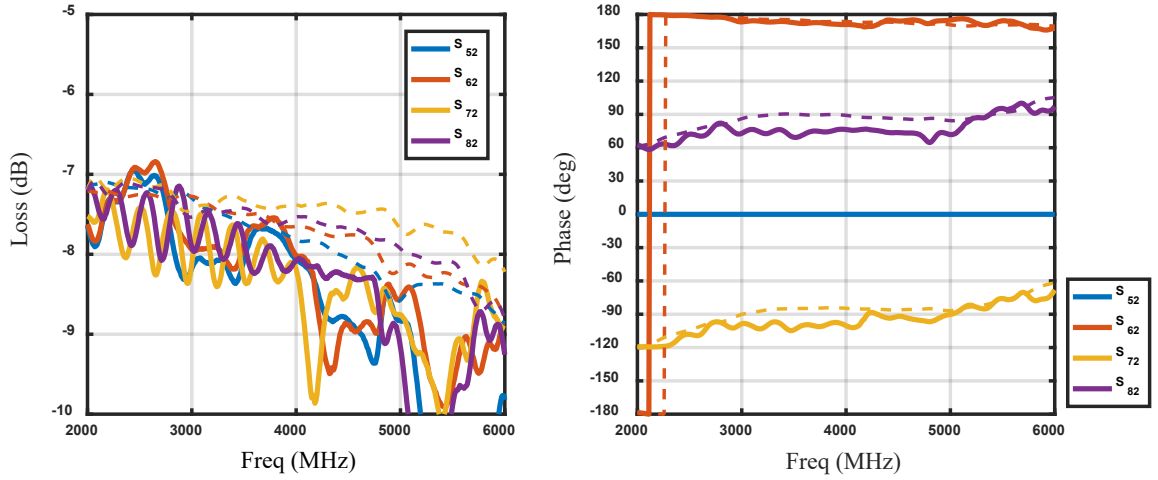

(b) Insertion loss and relative phases between input port 2 and output ports 5 – 8.

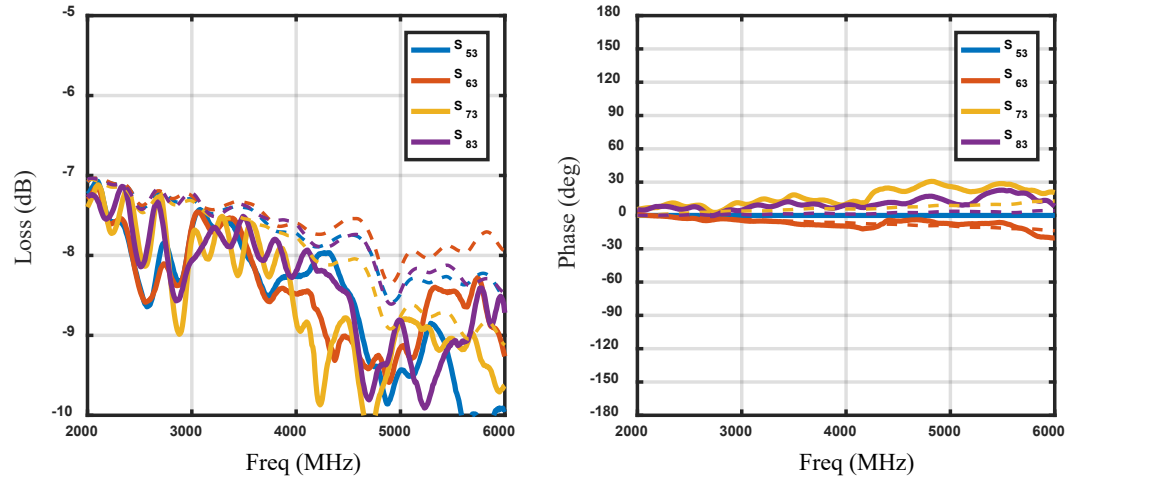

(c) Insertion loss and relative phases between input port 3 and output ports 5 – 8.

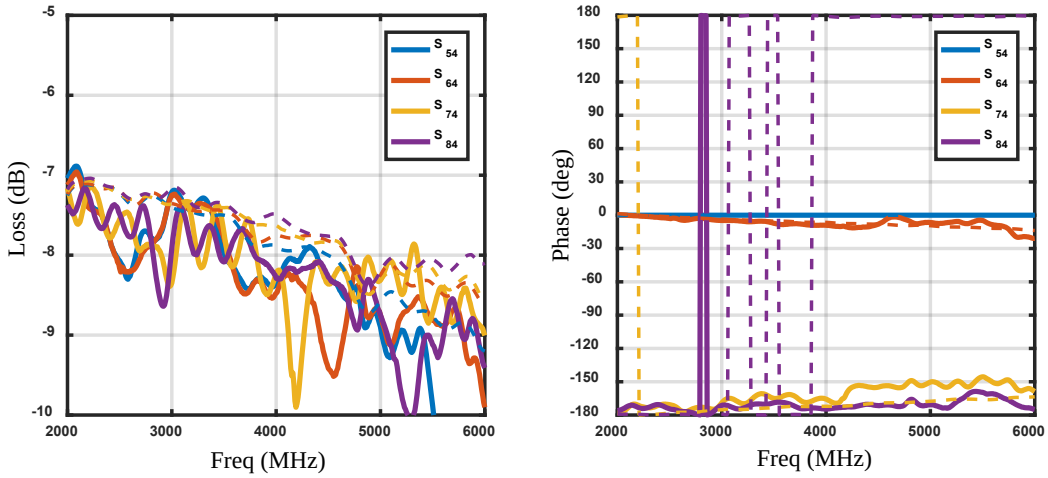

(d) Insertion loss and relative phases between input port 4 and output ports 5 – 8.

Figure 2-5: Insertion loss and relative phase for Board A.

Figure 2-6 shows the insertion loss (amplitude and phase) of Board B. The overall performance of Board B was better than Board A and closer to the modeled performance generated in Genesys. In this case, the difference between the measured and modeled phases was less than ±5° and the phase is observed to remain flatter across the frequency range from 3000 MHz to 5000 MHz – a 2 GHz band (a 50% bandwidth).

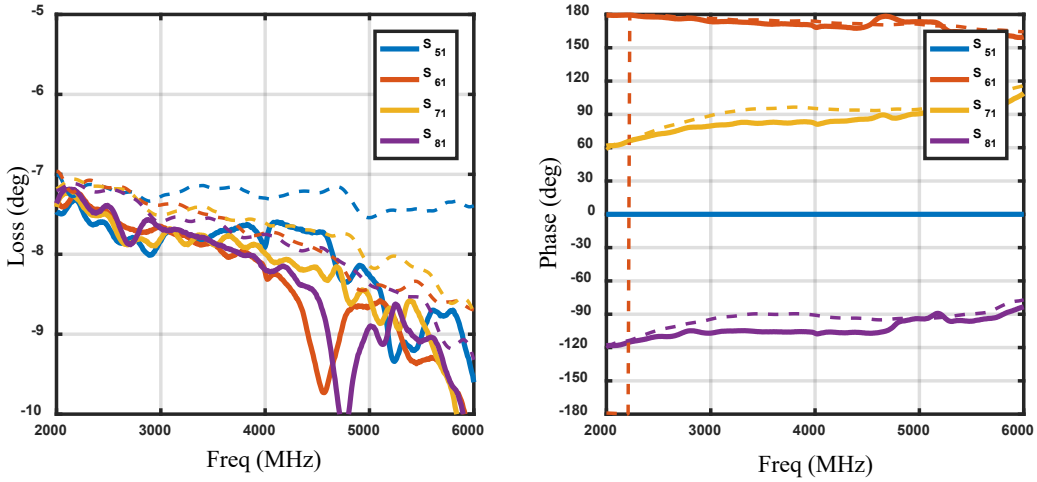

(a) Insertion loss and relative phases between input port 1 and output ports 5 – 8.

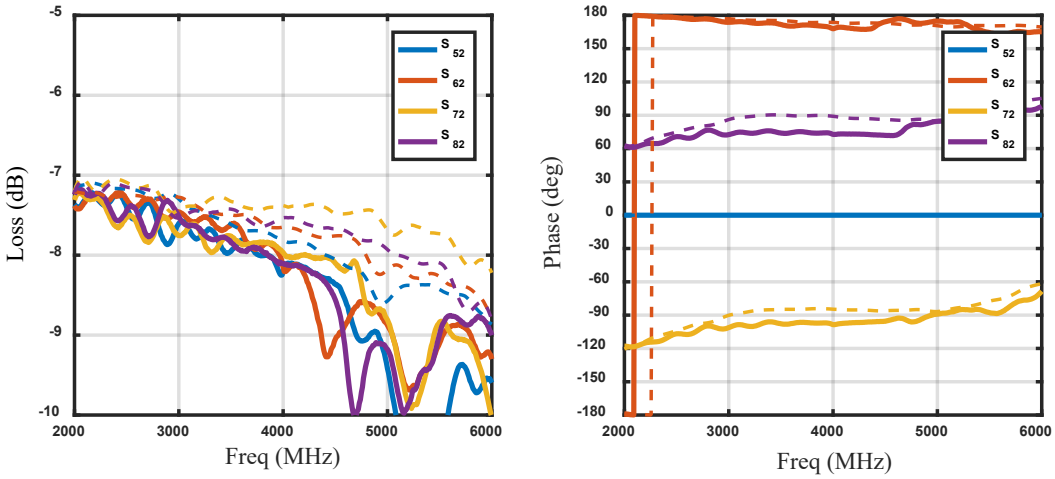

(b) Insertion loss and relative phases between input port 2 and output ports 5 – 8.

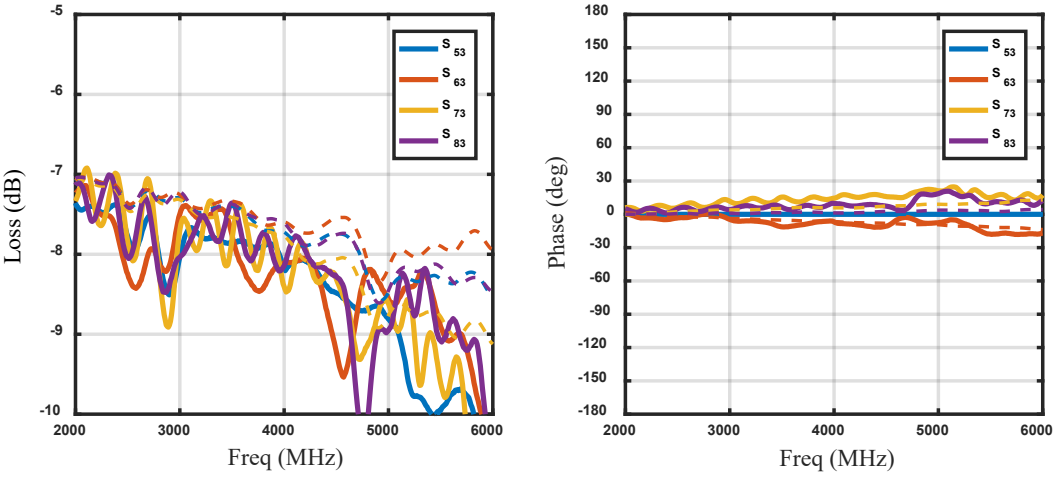

(c) Insertion loss and relative phases between input port 3 and output ports 5 – 8.

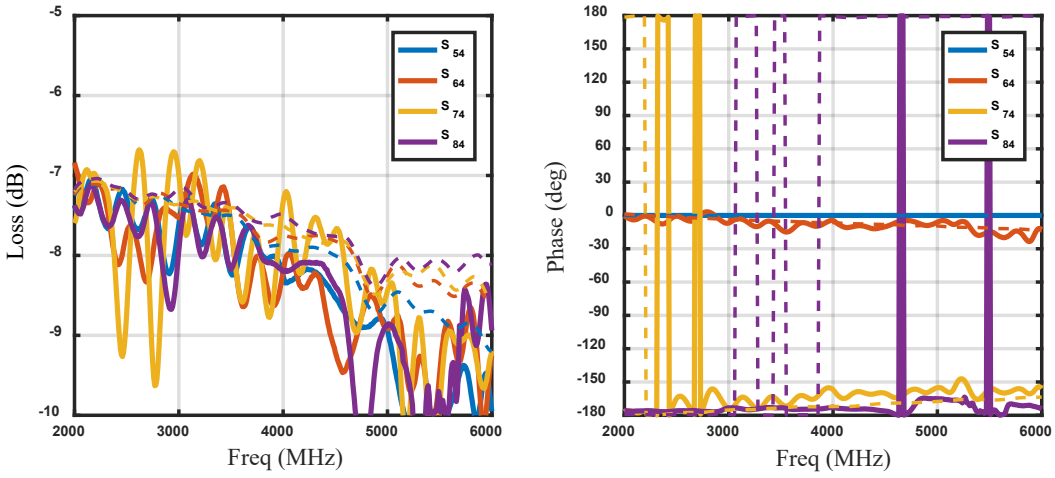

(d) Insertion loss and relative phases between input port 4 and output ports 5 – 8.

Figure 2-6: Insertion loss and relative phase for Board B.

Using the lessons learned from the 4 × 4 circuit board, we designed and built an 8 × 8 Butler matrix. As an example of a lesson learned, we updated the circuit board design to include vias under the 180-deg hybrids. The bottom side of the 180-deg hybrid is the ground plane while the top side of the circuit board is floating unless it is tied to the ground plane on the bottom of the circuit card. This connection is made using vias. These vias were not included in the 4 × 4 board.

The measured performance of the new 8 × 8 board requires further analysis and will be presented in a later report. However, in the next section, we will look at the modeled 8 X 8 Butler matrix data and use this data along with an element from an 8-element array to form directional beams as well as wideband nulls.

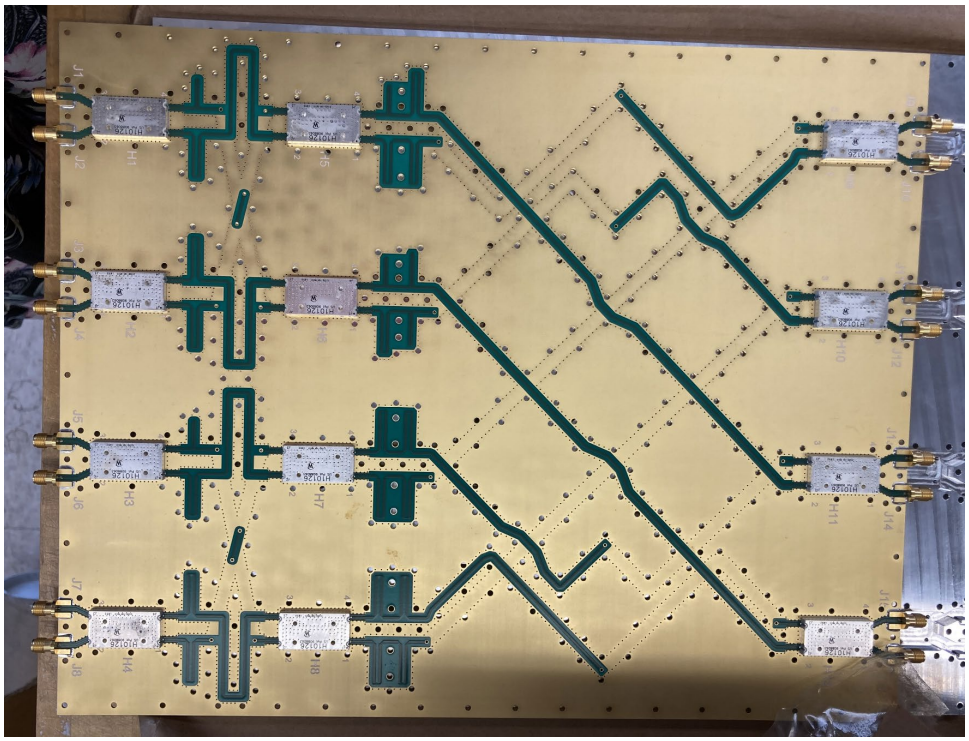

(a) Top view of the 8 X 8 Butler matrix circuit card.

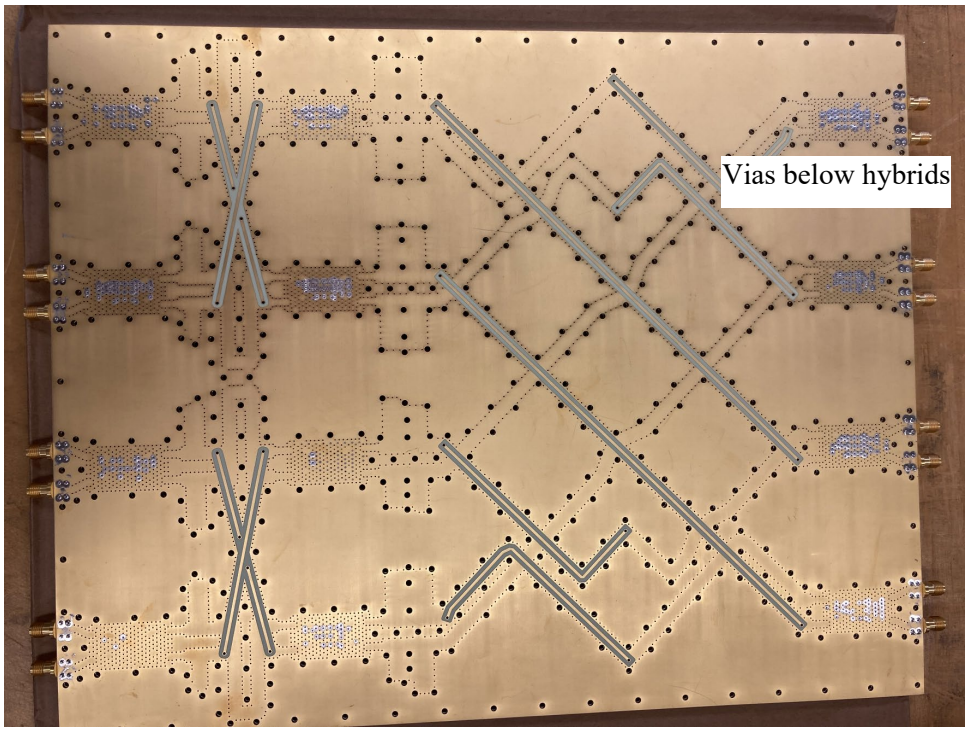

(b) Bottom view of the 8 X 8 Butler matrix

Figure 2-7: (a) Top and (b) bottom view of the 8 X 8 Butler matrix.

3. BEAMFORMING WITH PHASE MODES

In this section, we discuss the steps to generate phase modes from the radiating elements of a circular phased array. Figure 3-1 shows an AutoCAD drawing of the 8×8 Butler matrix. The basis of the 8×8 Butler matrix is the earlier 4×4 Butler matrix design. Two 4×4 Butler matrices are cascaded together and the outputs combined with additional phase shifters to form eight output beams.

The number of hybrids in an N-port Butler matrix is determined from Eq. (1) as:

$$N_{hybrids} = \frac{Nn}{2} \tag{1}$$

where N is the number of inputs and n is the number of rows determined from $N = 2^n$. In the same manner, the number of phase shifters, for the k^{th} row is determined from Eq. (2) as:

$$N_{phaseshifters} = \frac{N}{2} - 2^{k-1} \tag{2}$$

The details of a Butler matrix design to form phase modes are discussed in [1] and are based on the equations in [5].

Finally, we designed an 8-port crossover to connect the outputs from the phase shifters to four 180-deg hybrids. We designed the 8-port crossover on a 2-layer board to keep manufacturing costs low. Each of the eight paths of the crossover need to have an equal path loss to ensure that the crossover does not introduce large phases into the Butler matrix. This requirement was satisfied by ensuring that the optimized group delay was maintained within ±5 picoseconds for all the paths. Details of the design of the crossover are in [3].

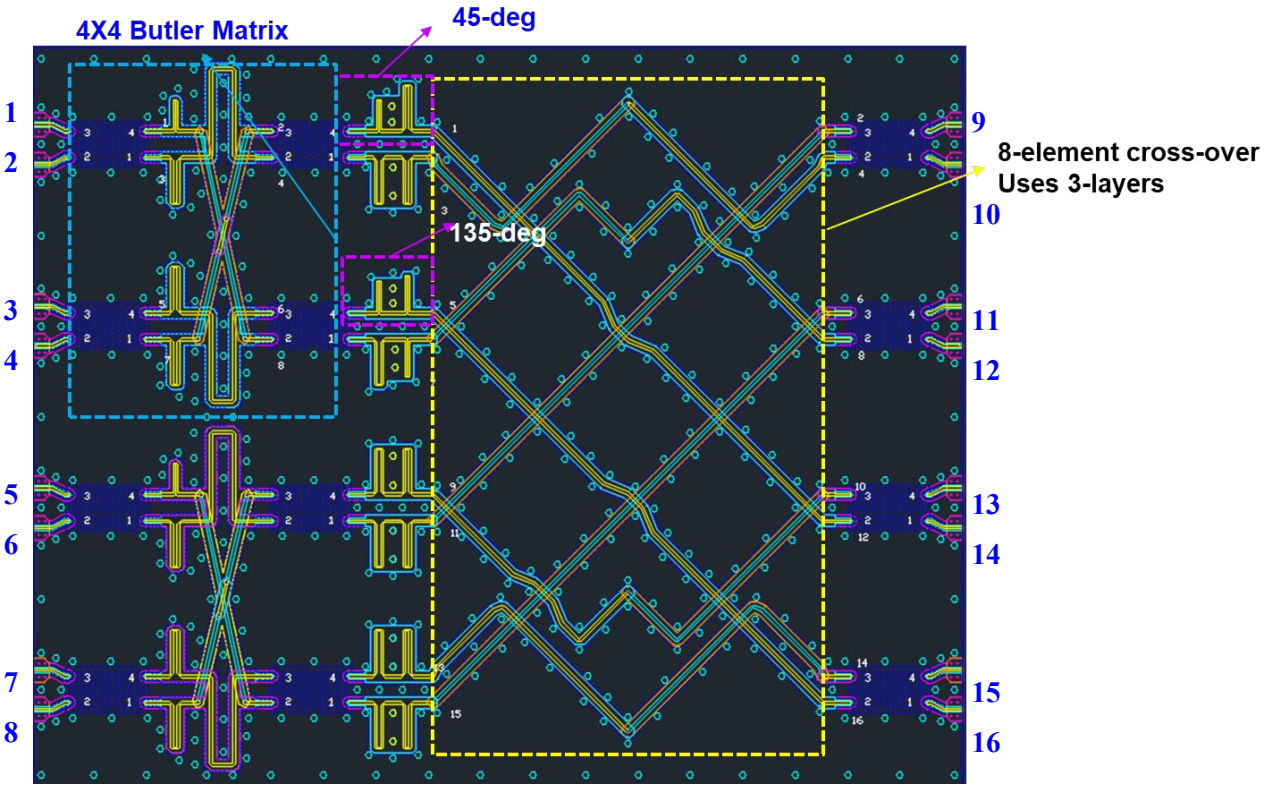

Figure 3-1: AutoCAD layout of the 8 X 8 Butler matrix. Each component was individually designed in Ansys HFSS™ and then the layout done in AutoCAD. The numbers in blue indicate the input (1-8) and output (9-16) port numbers. The magenta boxes show an example of a 45-deg and 135-deg phase shifter, while the blue box shows the 4 X 4 Butler matrix.

Figure 3-2 shows simulated results for the 8×8 Butler matrix, using the port numbering scheme from Figure 3-1. The input ports range from 1 to 8, and the output ports range from 9 to 16. The following observations are made:

- The insertion loss tended to increase at the higher end of the band, but between 2 GHz and 4 GHz, the losses across the different paths remain steady and with relatively small differences between the various paths.
- The relative phase remains within ±5° for the various paths.

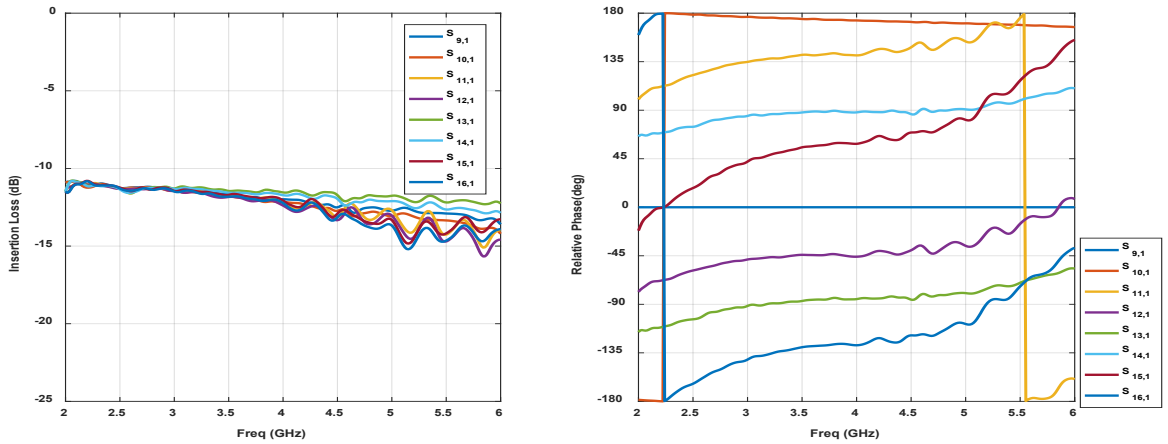

(a) Insertion loss and relative phase for the case when the input port is 1 and the output ports are 9 – 16

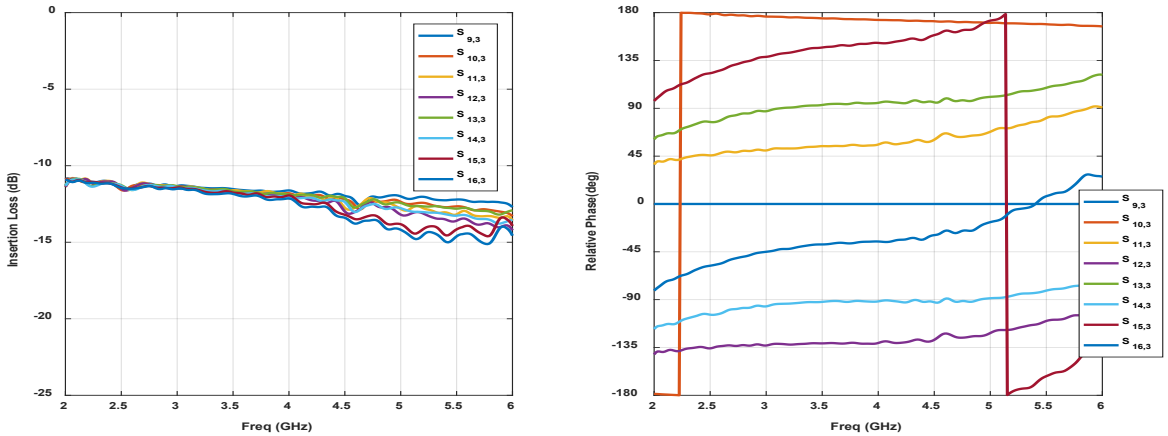

(b) Insertion loss and relative phase for the case when the input port is 3 and the output ports are 9 – 16

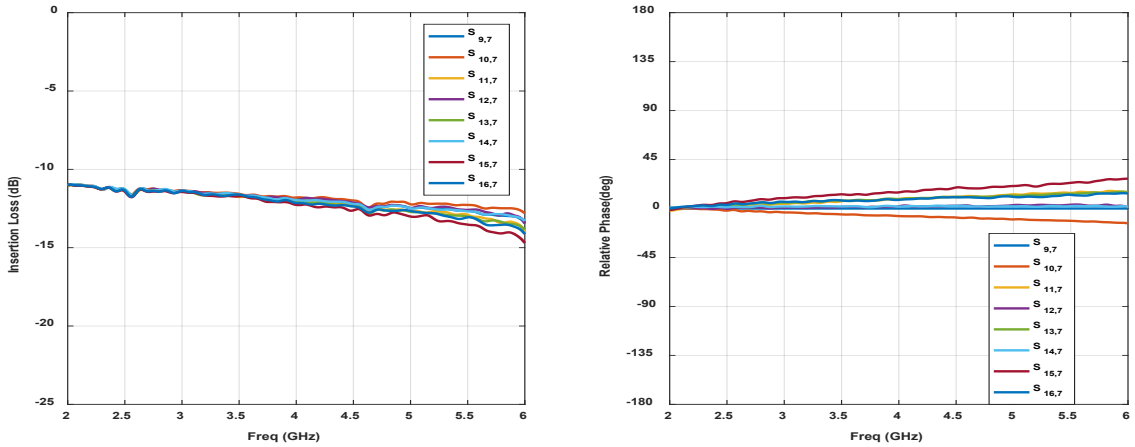

(c) Insertion loss and relative phase when the input port is 7 and the output ports are 9 – 16

Figure 3-2: Insertion loss and relative phase for a subset of input and output ports for the modeled 8 X 8 Butler matrix are shown. The components of the Butler matrix were designed and optimized in Ansys HFSS™ and then imported into Genesys for the simulation of the overall design.

3.1 Modal Beamformer

We modeled the formation of phase modes using the 8×8 Butler matrix model. We limit the presentation of results to an 8×8 model, in this research, as we were not able to build a larger matrix in the time allotted for this 6.2 effort. However, the presented results are easily scaled to Butler matrices of larger sizes. In the following sections, we introduce a simple 8-element circular array designed using stepped notch elements, and demonstrate the formation of phase modes. We then show how these phase modes are phased and weighted to form directional beams with and without nulls over 2 GHz of band.

We reconsider the architecture of a simple phase mode beamformer. Figure 3-3 shows the architecture of a phase mode beamformer. The inputs to the modal beamformer are the circular array elements while the outputs are the phase modes. A modal beamformer has two functional blocks: an N -point Discrete Fourier Transform (DFT) block and an equalizer block. A quick overview of how phase modes simplify beamforming for circular arrays is discussed next.

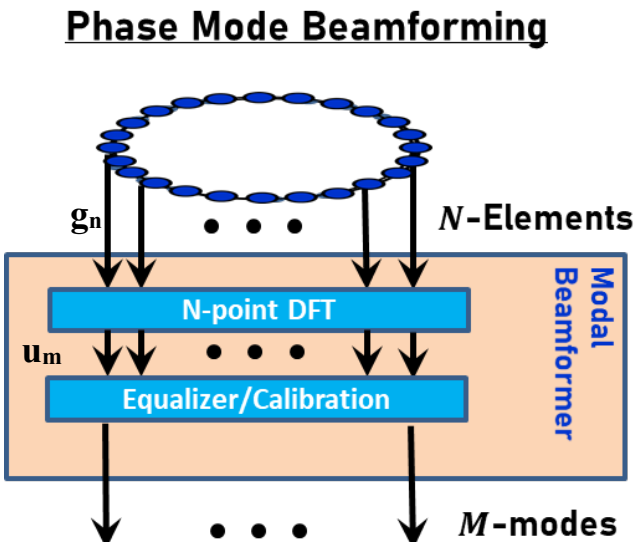

Figure 3-3: A simple architecture of a modal beamformer. The inputs to a modal beamformer are the circular radiating elements and the output are phase modes. $\boldsymbol{N}$ elements produce up to $\boldsymbol{M}$ phase modes where $\boldsymbol{M} \leq \boldsymbol{N}$.

Consider a circular array, as shown in Figure 3-3, with N elements uniformly spaced on a circle of radius a. The radiation field pattern, $g_n(\phi)$, of the nth element is dependent on the rotation of the element.

$$g_n(\phi) = g_o\left(\phi - \frac{2\pi n}{N}\right) \tag{3}$$

In conventional beamforming, where the weights are set for each element at every scan angle, the final radiation pattern is given by:

$$F(\phi) = \sum w_n g_n(\phi) e^{jkacos(\phi - \phi_n)} \tag{4}$$

As discussed before, this methodology is intimately dependent on the element's rotation, which has to be taken into account when generating weights for beamforming. With the use of phase modes, it is possible to simplify this calculation and make it independent of the element's rotation. There is the added advantage

of frequency invariance that is obtained with this approach. Using the relationship where an exponent is written as a sum of Bessel functions of the first kind,

$$e^{jkacos\,\phi} = \sum_v j^v J_v(ka) e^{jv\phi}. \quad (5)$$

And defining the FFT block operations using N orthonormal phase modes as

$$\Phi_m^{transpose} = \frac{1}{\sqrt{N}}\left(1, e^{-j\left(\frac{2\pi m}{N}\right)}, e^{-j2\left(\frac{2\pi m}{N}\right)}, \dots, e^{-j(N-1)\left(\frac{2\pi m}{N}\right)}\right). \quad (6)$$

The phase mode at the output of the FFT block is then as shown in Eq. (7). The details of this calculation are in Ref. [2].

$$u_m = \left[A_m(ka) + \underbrace{\delta A_m(ka, \phi)}_{\sim 0}\right] e^{jm\phi} = A_m(ka) e^{jm\phi} \quad (7)$$

Even though the elements have slight variations with frequency, the equalization/calibration block is used to calibrate out these variations. We will detail the equalization block in a future report. After equalization, the final radiation pattern, independent of frequency, is simply written as

$$F_{out} = \sum_m a_m e^{jm(\phi - \phi_m)}. \quad (8)$$

Setting the appropriate amplitude and weight at the phase mode level will control sidelobes and scan the beam.

3.2 8-Element Circular Array

To verify the performance of the 8×8 Butler matrix design and generate phase modes, the first step is to have embedded element patterns; these can be obtained from an HFSS model. For this work, we designed an 8-element array consisting of stepped notch elements. These elements were optimized to operate over a frequency band of 2 GHz to 6 GHz. Figure 3-4 shows the unit cell of an element of this array as well as its S_{11} or reflection coefficient. Between the frequency ranges of 2 GHz to 6 GHz, the reflection coefficient, of the unit cell, remains below -10 dB.

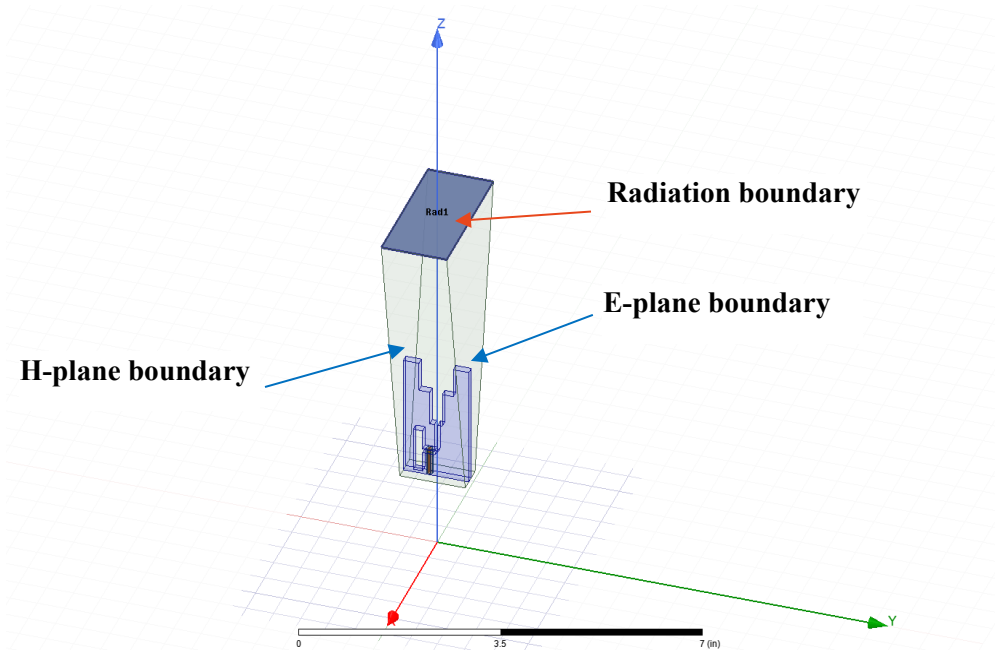

(a) Unit cell in wedge periodic boundary conditions. The top of the box is the radiation boundary while the x-z planes are the H-plane boundaries.

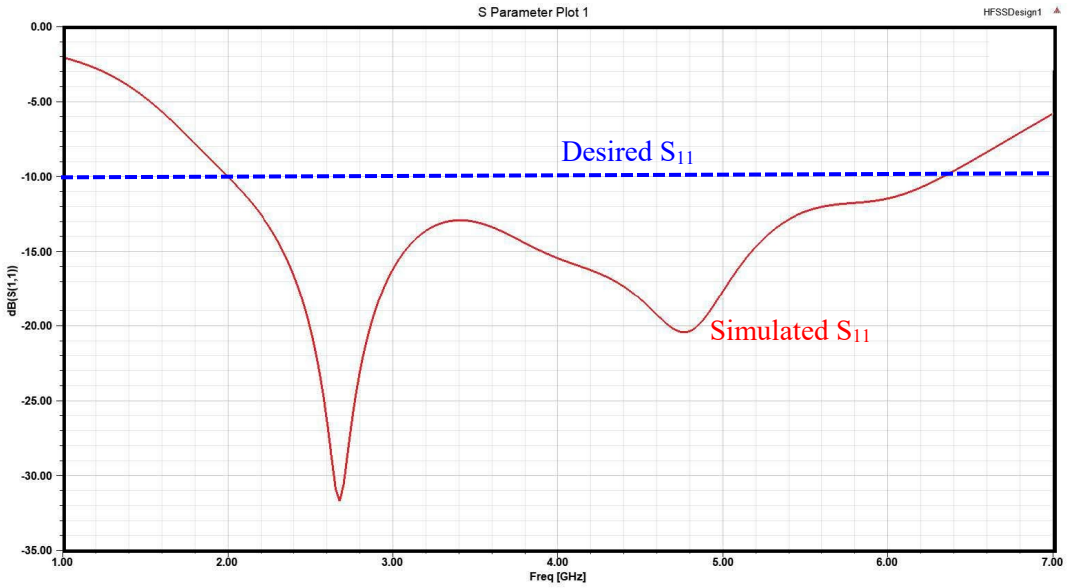

(b) The S_{11} of the stepped notch element over the frequency range from 1 GHz to 7 GHz.

Figure 3-4: The unit-cell of an 8-element array and its reflection loss over a 1GHz to 7 GHz frequency band

Figure 3-5 shows the full 8-element circular array constructed from the unit cell shown in Figure 3-4. Note that only the outside surfaces, as indicated in Figure 3-5, are radiation boundaries (indicated by rad1). The top and bottom surfaces of the model are E-plane boundaries. Using E-plane boundaries allows us to model an infinite array of stepped notch elements in the vertical direction (imagine a cylindrical array).

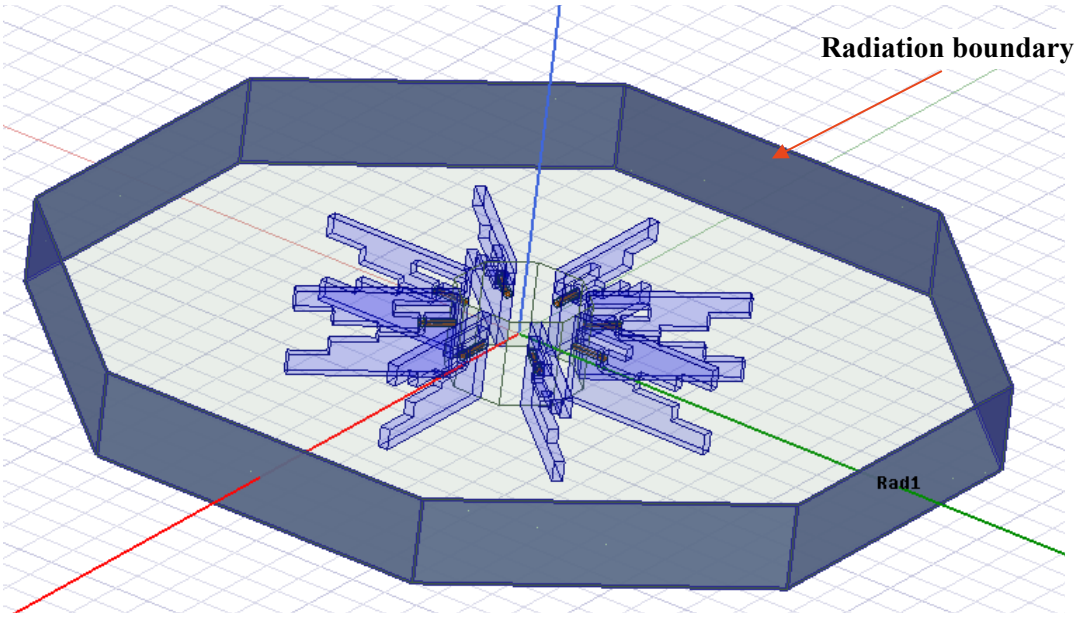

Figure 3-5: A model of an 8-element circular array using stepped notch elements

An example of the radiation pattern for one of these stepped notch elements is shown in Figure 3-6. These plots are for frequencies ranging from 2GHz to 6GHz. Note, that after 5GHz, the element pattern starts degrading with the formation of shoulders. The overall pattern does not retain its cosine shape at the higher frequencies and "shoulders" begin to appear near boresight. This degradation of the pattern may be attributed to a resonance that appears in the S_{11} around 5.3 GHz, as seen in Figure 3-7.

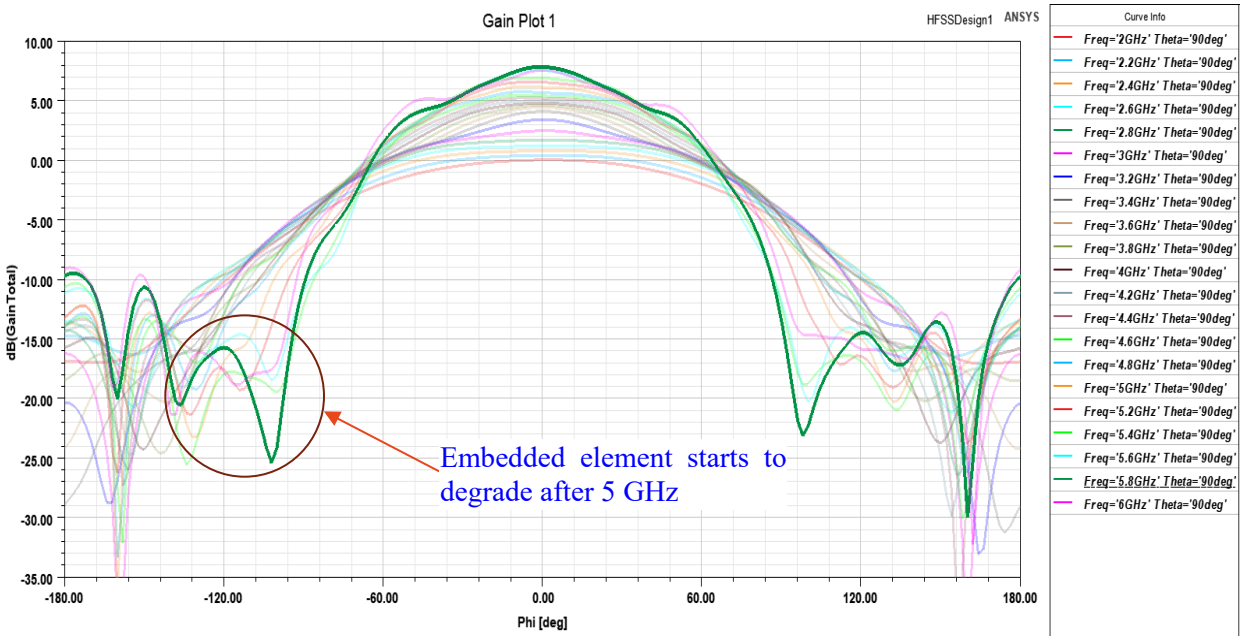

Figure 3-6: Embedded element pattern over the band of operation from 2 GHz to 6 GHz.

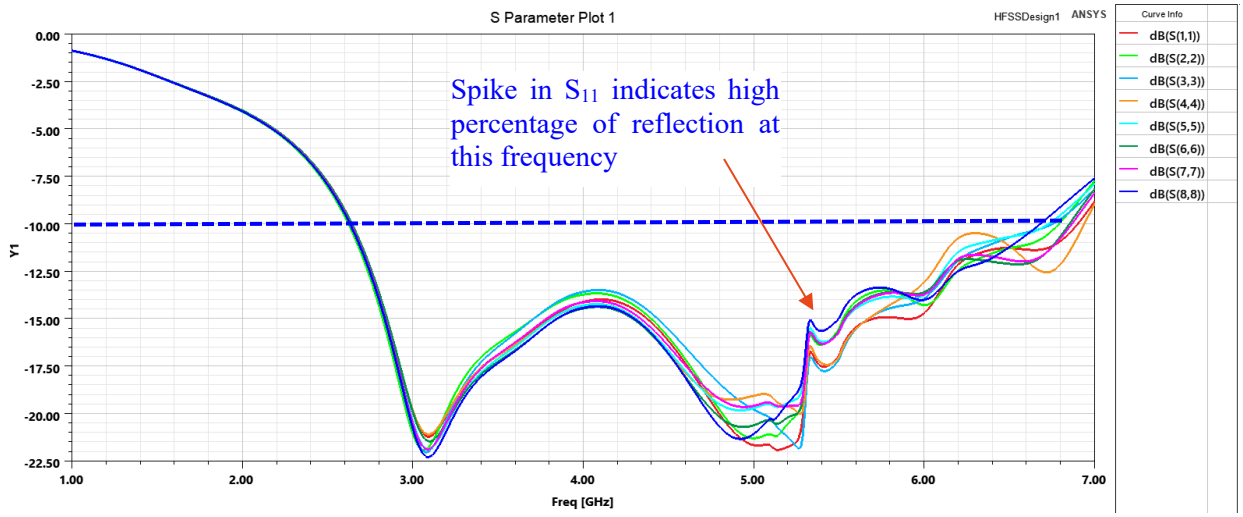

Figure 3-7: Reflection coefficient of an embedded element for frequencies ranging from 1 GHz to 7 GHz. A spike in S_{11} occurs at around 5.3 GHz.

3.3 Generation of Phase Modes

Using the architecture shown in Figure 3-3, Figure 3-8 shows how the antenna and Butler matrix circuit card are integrated together to generate phase modes. The inputs to the Butler matrix are the radiating elements of the circular array. The outputs of the Butler matrix are phase modes as shown in the same figure. Note that the phase modes are not generated in a uniform manner, i.e. at the first output port, a phase mode with three phase cycles is formed while at the second output port, a phase mode with one phase cycle is formed and the zeroth mode is formed at the 7^{th} output port. It is important to know which mode forms at which output to ensure that the correct phase shift is applied at the correct mode to form a scanned directional beam. This is analogous to applying the correct phase shift at the correct element of a linear array. The output port at which the other phase modes are formed are all shown in Figure 3-8.

Once these phase modes are formed, these phase modes need to be equalized such that the amplitudes are equal across all the modes and the phase starts at zero. The equalization steps are shown in Figure 3-9. Each of the phase mode uses a time delay line, attenuators and phase shifters to equalize the phase modes across the desired frequency of operation. The details of these equalization steps and performance is in [6].

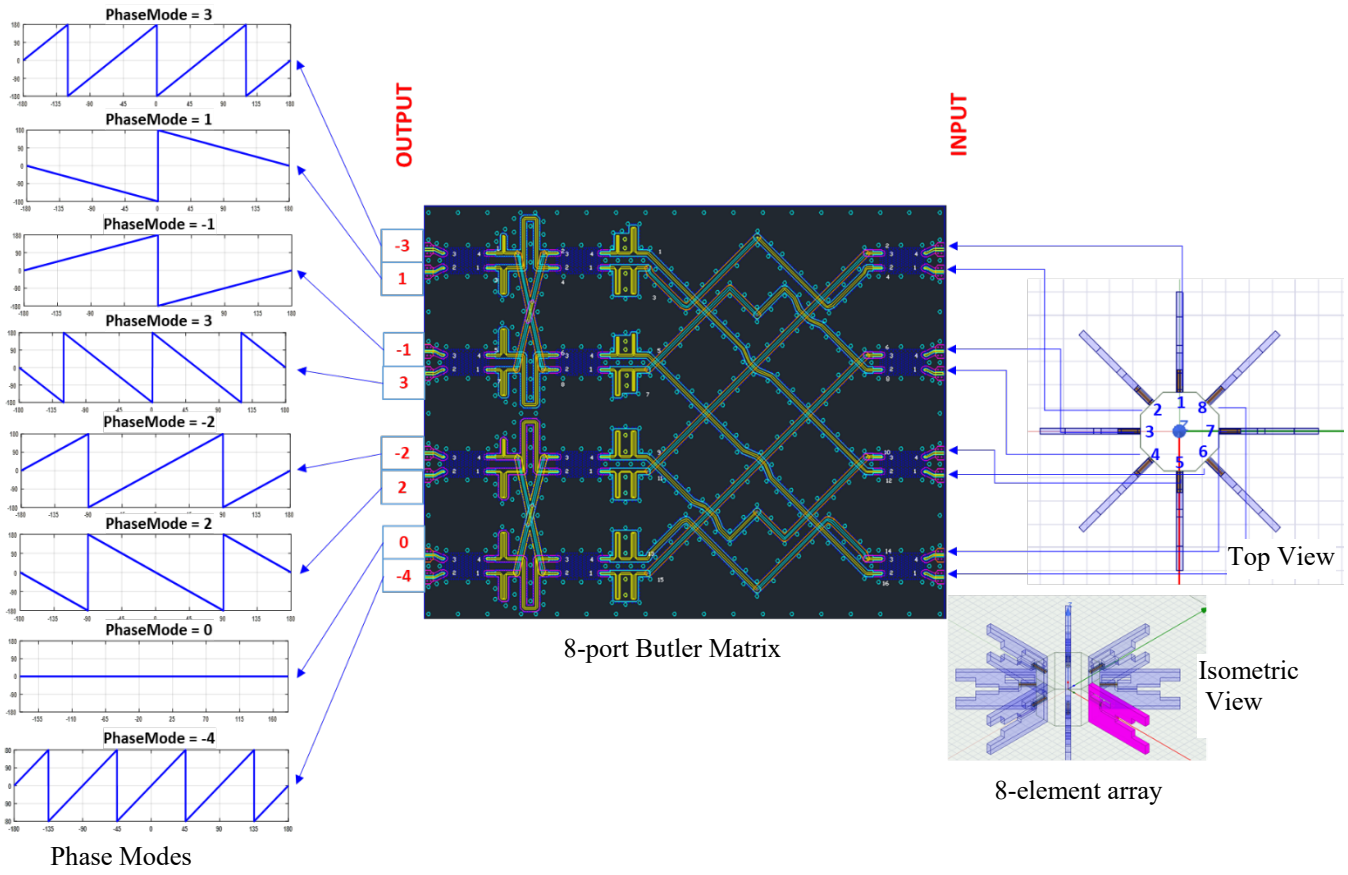

Figure 3-8: The block diagram to generate the phase modes from a circular array's radiating elements and a Butler matrix.

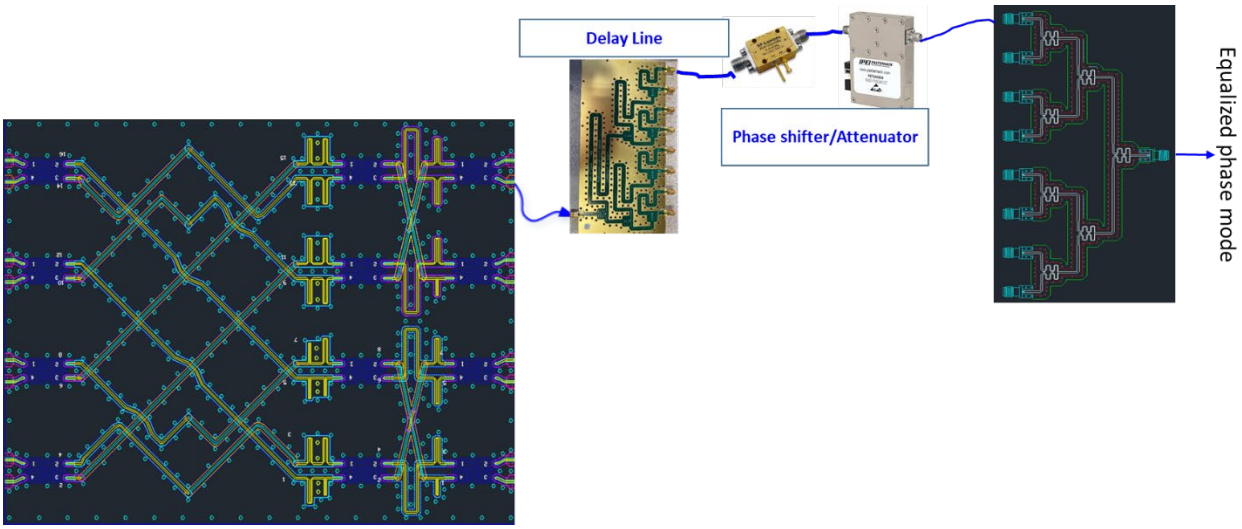

Figure 3-9: Equalizing phase modes before beamforming.

Another interesting feature of the modal beamformer is the following: if the formed phase modes are added using an 8-way combiner, then the output is the embedded element pattern once again. This arrangement is

shown in Figure 3-10. As an example, the case of the embedded element pattern at 3.0 GHz is shown. The green curve at the output is the embedded element pattern formed by summing the phase modes. The input and output patterns are relatively close except for ripples in the final patterns that do not exist in the starting radiation patterns. These are due to amplitude/phase errors of the designed circuit card.

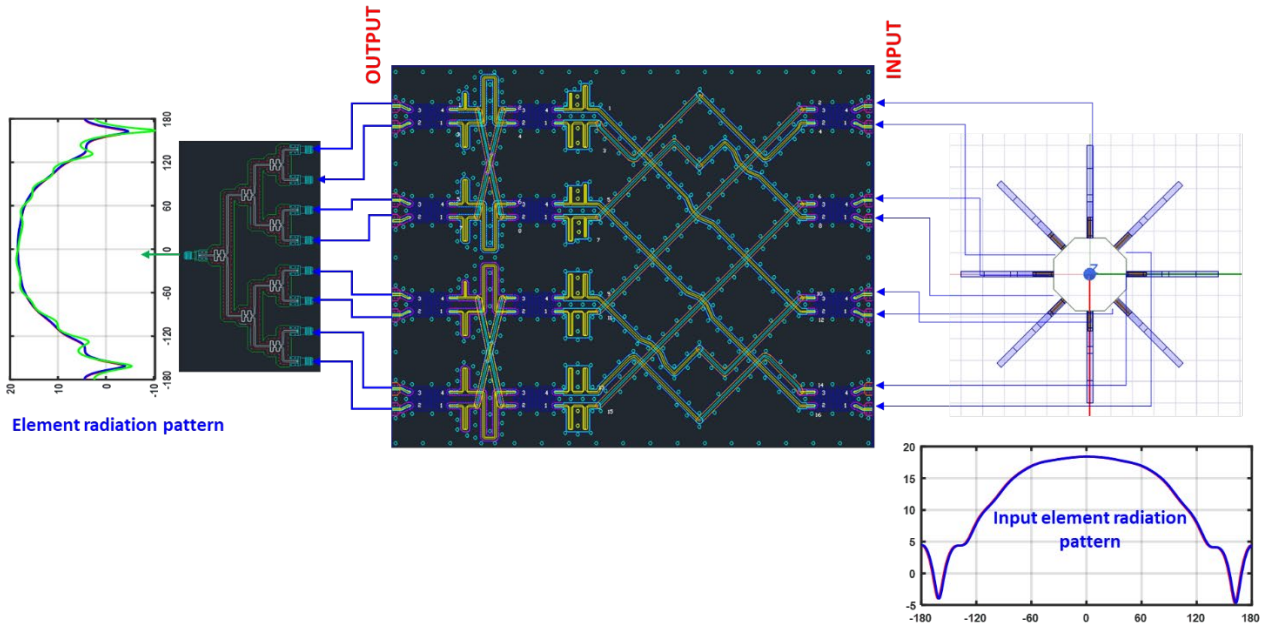

Figure 3-10: Forming an element radiation pattern using a phase modal beamformer.

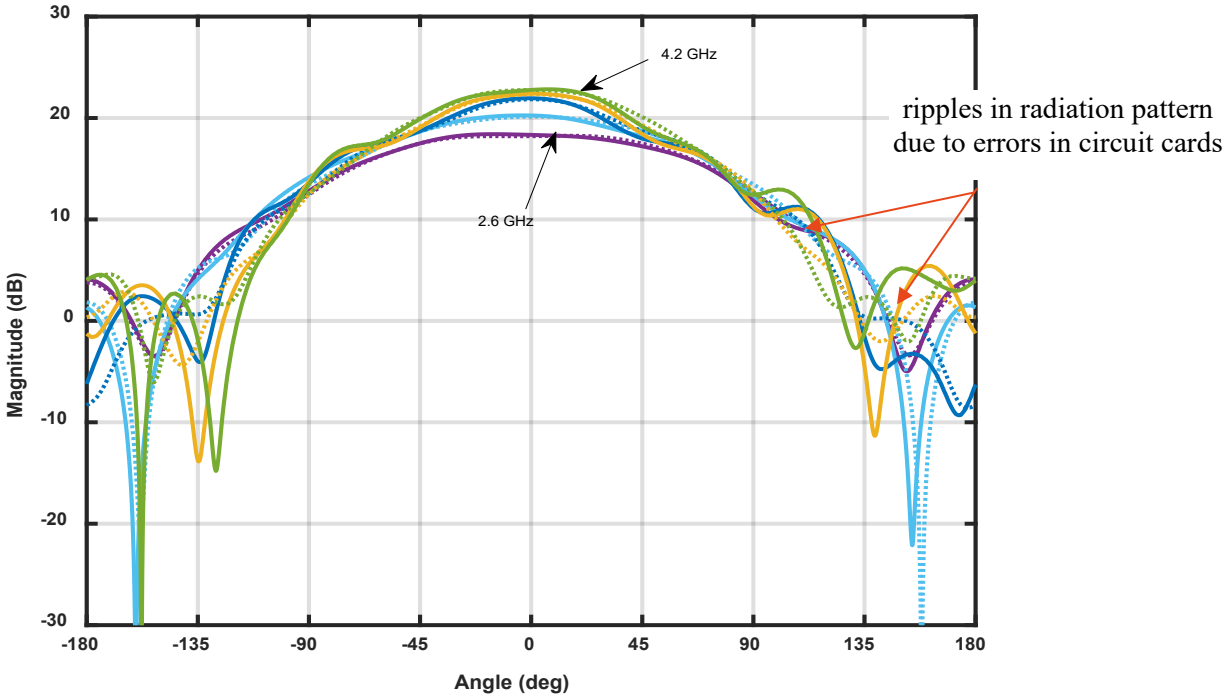

Figure 3-11: Embedded element radiation from HFSS (dashed) and from beamformer (solid) for frequencies from 2.6 GHz to 4.2 GHz with a resolution of 0.4 GHz.

3.4 Directional Beamforming

In this section, we look at how the equalized phase modes are used to form directional beams as well as beams with nulls. Before forming these directional beams, we consider the generated, equalized phase modes at four different frequencies: 2.6 GHz, 3.0 GHz, 3.4 GHz, 3.8 GHz and 4.2 GHz. Figure 3-12 shows the phases for the modes at these five frequencies. Note that after equalization the shapes of the plots are similar, i.e. the number of cycles follows the phase mode but the jumps in the phase differ from frequency to frequency. There are also ripples in the plots, which are a result of the inherent errors present in the board itself.

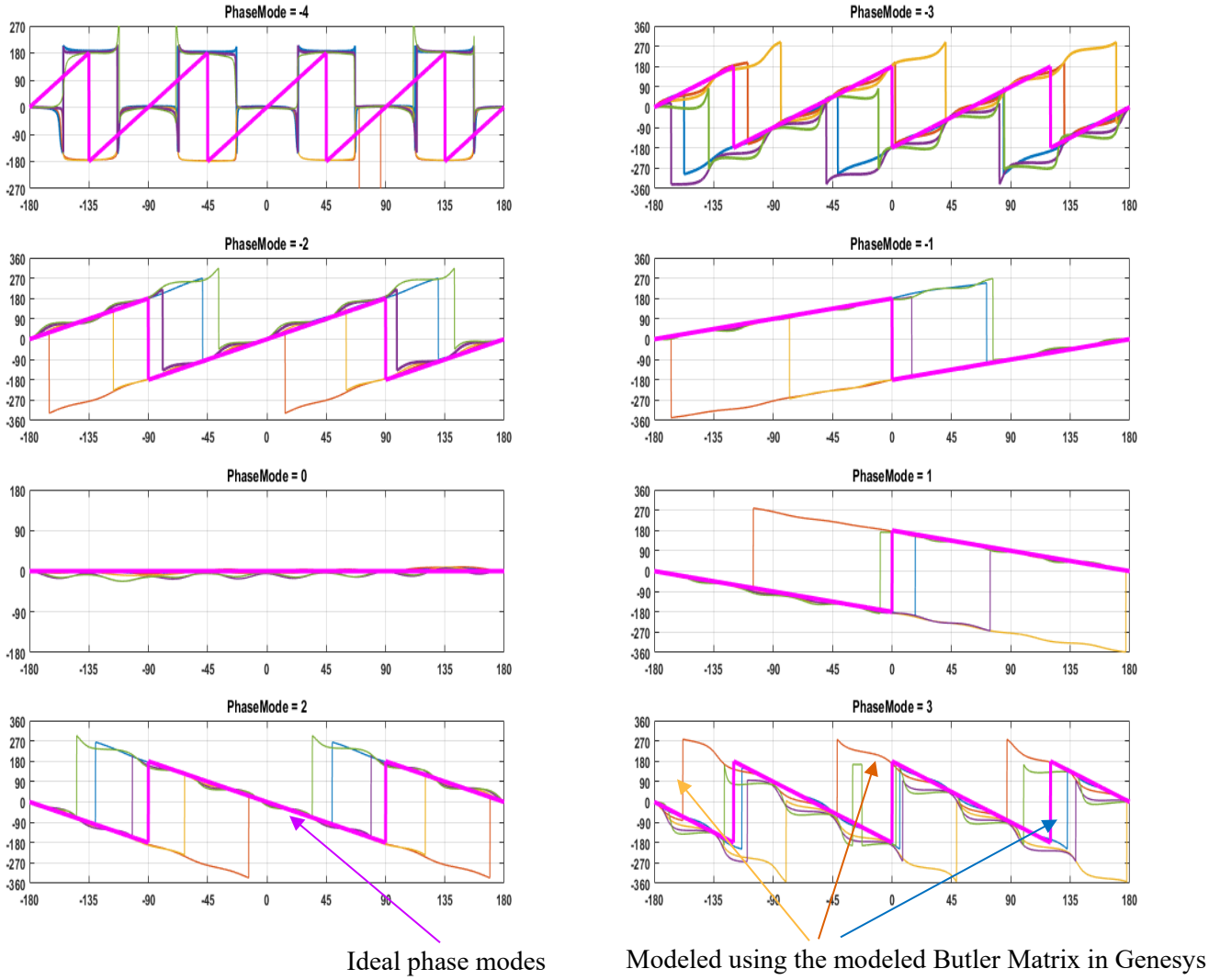

Figure 3-12: Phase modes (ideal and simulated). The simulated phase modes are shown for five different frequencies. Note the ripples in the phase are due to phase error inherent in the circuit card.

Using these generated phase modes, we form a directional beam with its main beam pointed at $\phi = 0^o$ for frequencies ranging from 2.6GHz to 4.2GHz. Note, that with equalization, the beamwidths at the different

frequencies are almost identical. The identical beamwidths are an indication of the frequency invariance property of modal beamformers. Another example of a radiation pattern where the main beam is steered to 30^{O} is shown in Figure 3-14. Since this is a small array with only eight elements and there are inherent errors in the modal beamformer, the sidelobes here are not well maintained, but the main beam remains about the same across the band.

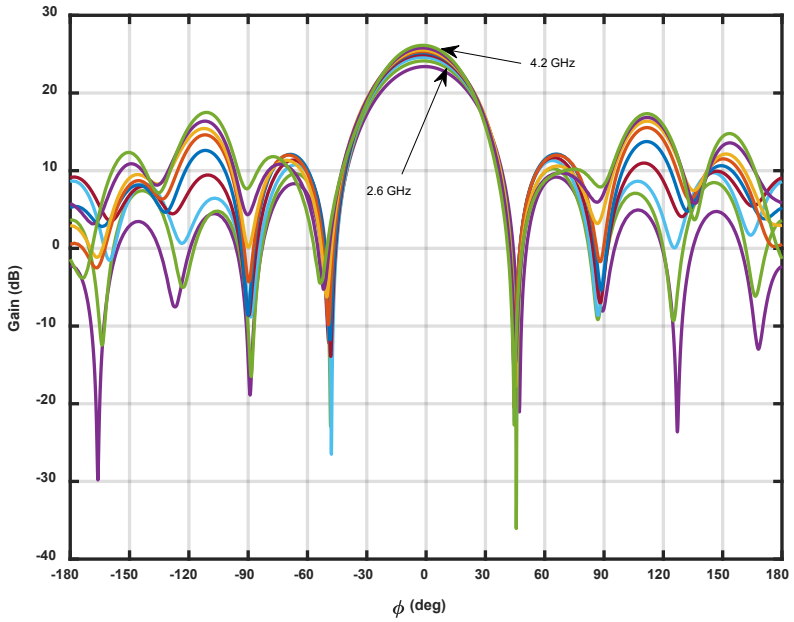

Figure 3-13: A directional beam formed using 8 phase modes for frequencies ranging from 2.6 GHz to 4.2 GHz spaced 0.2 GHz apart.

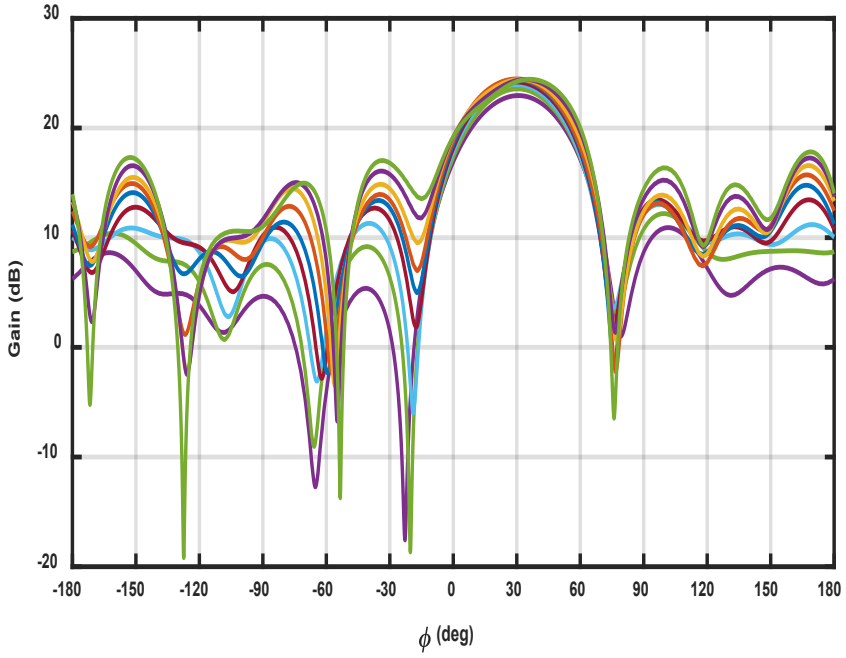

Figure 3-14: A directional beam pointed at 30^{O} is formed from phase modes. These radiation plots are from frequencies ranging from 2.6 GHz to 4.2 GHz spaced 0.2 GHz.

Next, we form a null in the directional beam. In Figure 3-15, the directional beam is at $\phi = 0^o$ with a null formed at $\phi = 60^o$.

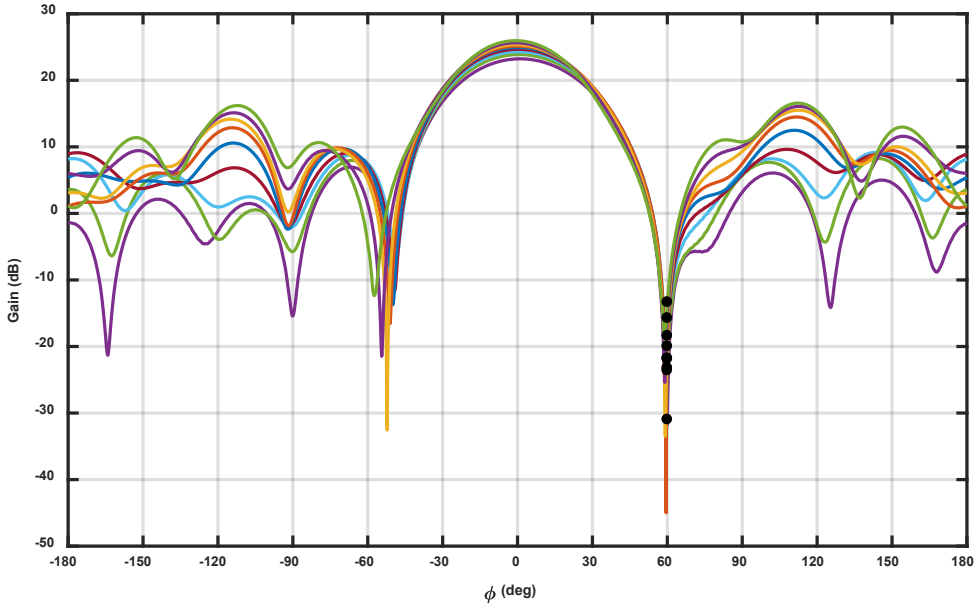

Figure 3-15: A directional beam with a null at 60° using a modal beamformer. The frequencies considered range from 2.6 GHz to 4.2 GHz with a 0.2 GHz resolution.

For the final example of modal beamforming, we looked at a 16-element array made of stepped notch elements as shown in Figure 3-16.

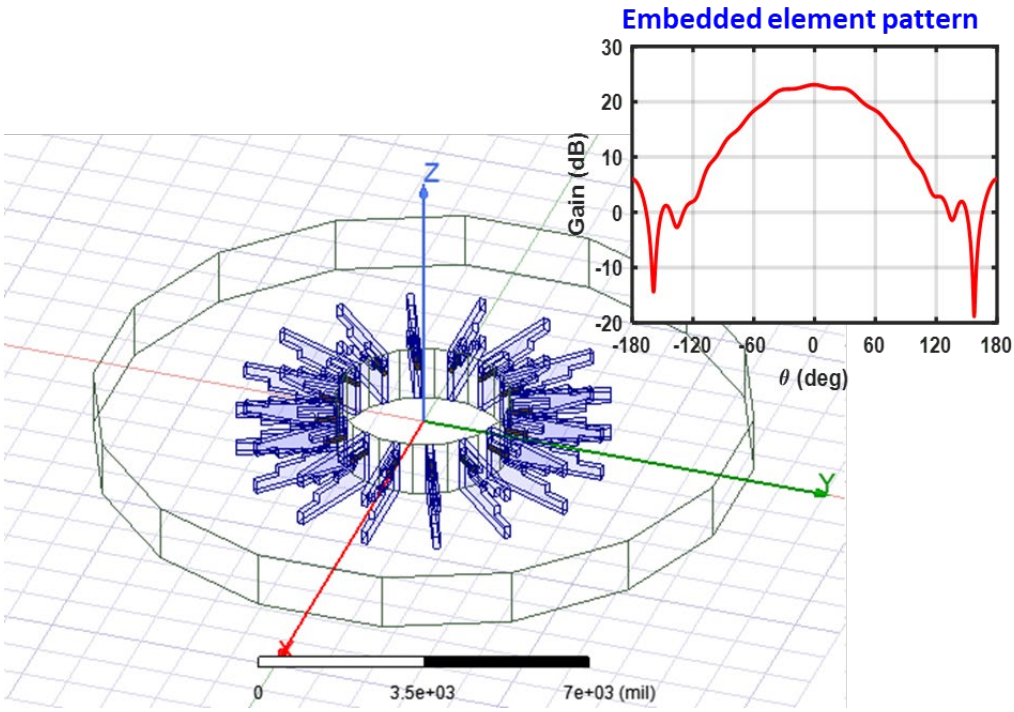

Figure 3-16: A 16-element circular array made of stepped notch elements and spaced at 22.5°.

For this example, we modeled a 16-port Butler matrix in Genesys. Figure 3-17 shows the layout of the simulation as modeled in Genesys. Each of the highlighted components (in red boxes) were designed and optimized in HFSS and the modeled S-parameters exported into Genesys to create the final model.

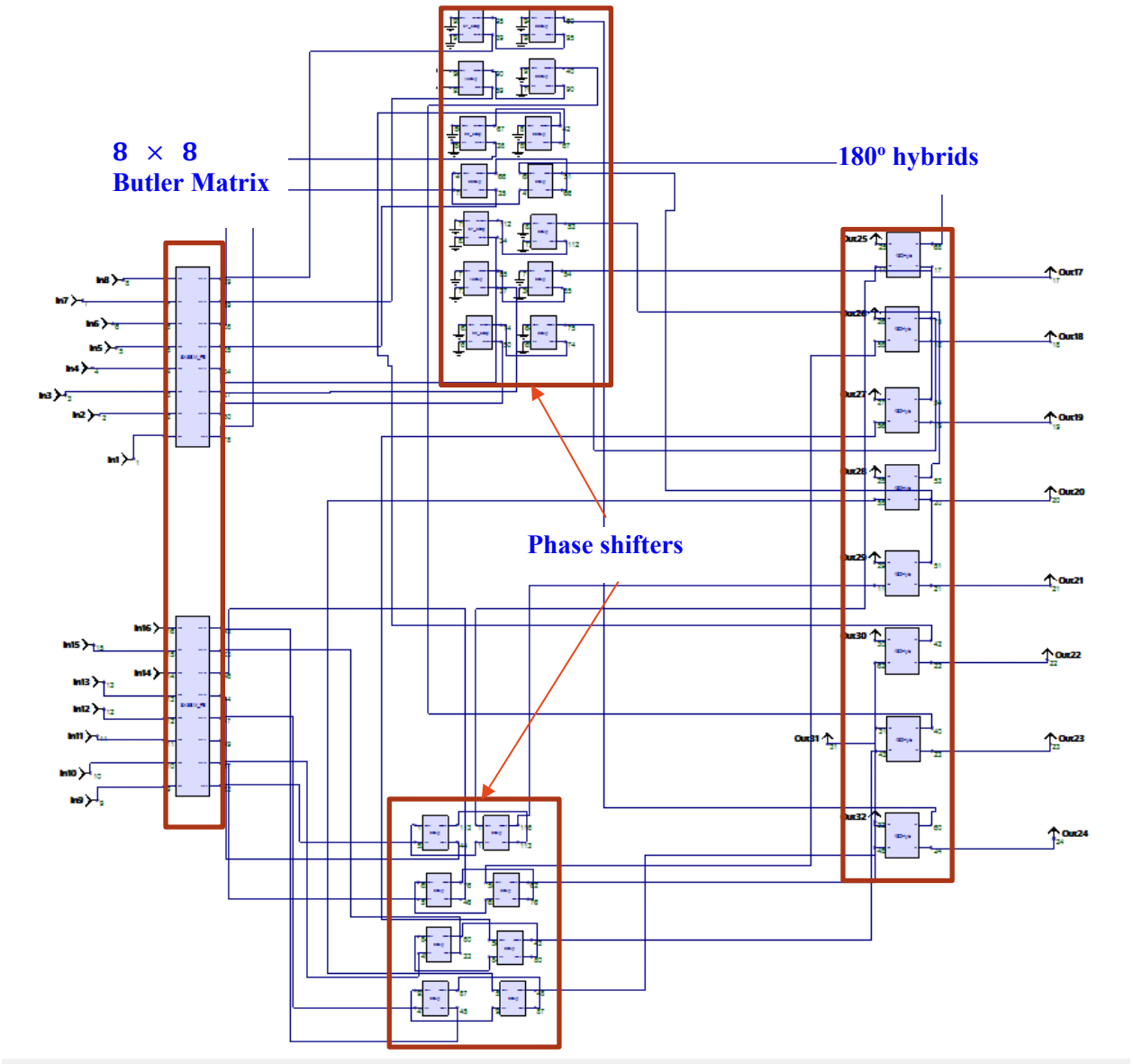

Figure 3-17: 16 X 16 Butler matrix made of components modeled in HFSS.

Figure 3-18 shows the phase modes of the 16-element design. These plots are at 4.5 GHz.

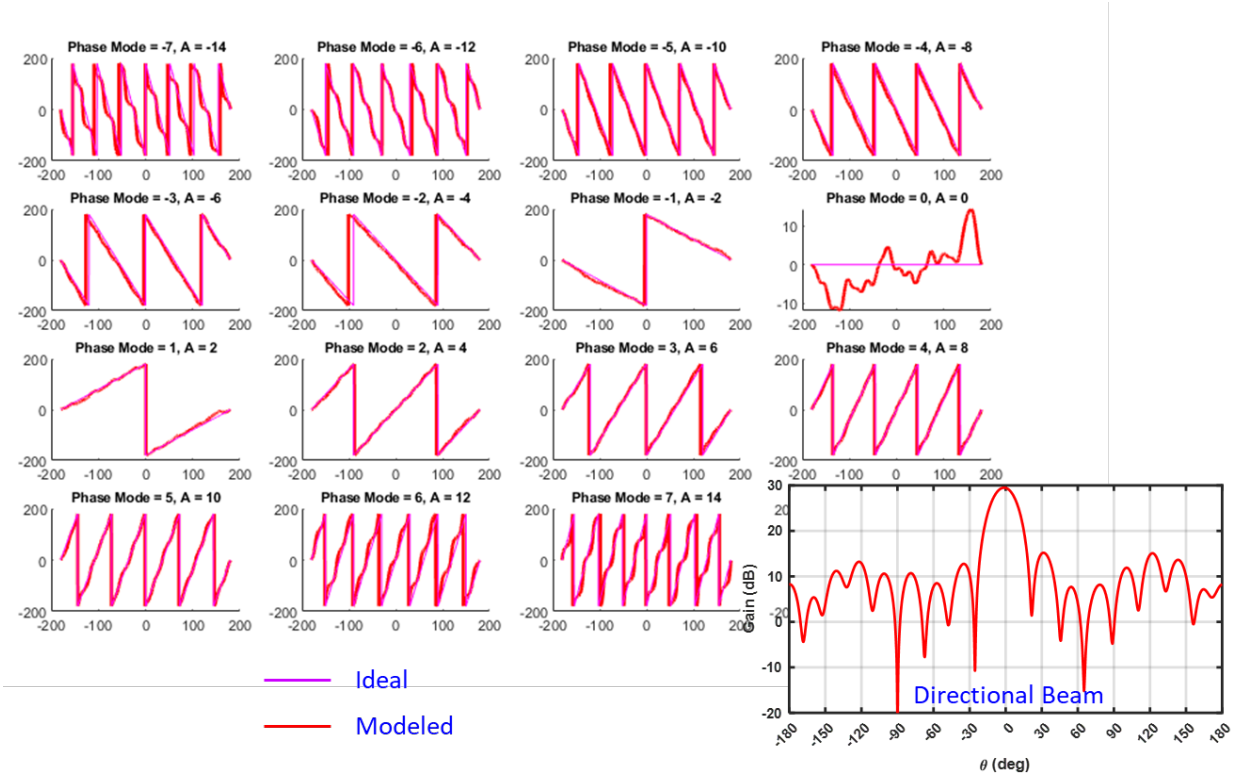

Figure 3-18: Example of modeled phase modes and directional beam from a 16-element circular array integrated with a 16-port Butler matrix.

For the next set of plots in Figure 3-19, we scanned the beam to -20º while forming a null at 60º. The plot in Figure 3-19(a) is at 4.5 GHz while the plots in Figure 3-19(b) are for frequencies ranging from 2.5 GHz to 4.5 GHz with a resolution of 0.5 GHz. For this case, we had a requirement to form one null at 60º while the main beam scanned to -20º. We used the null formation techniques outlined in [7] to form the nulls in these patterns.

Reference [7] has the details of the fast null formation techniques implemented here. Figure 3-19 (b) shows plots, before and after nulling, from minimum frequency of 2.5 GHz to maximum frequency of 4.5 GHz in 0.5 GHz steps. For all frequencies, the beamwidth of the radiation plots do not change, before or after nulling, across the band demonstrating the frequency invariance of modal beamforming. The null performance also remains constant at the higher frequencies.

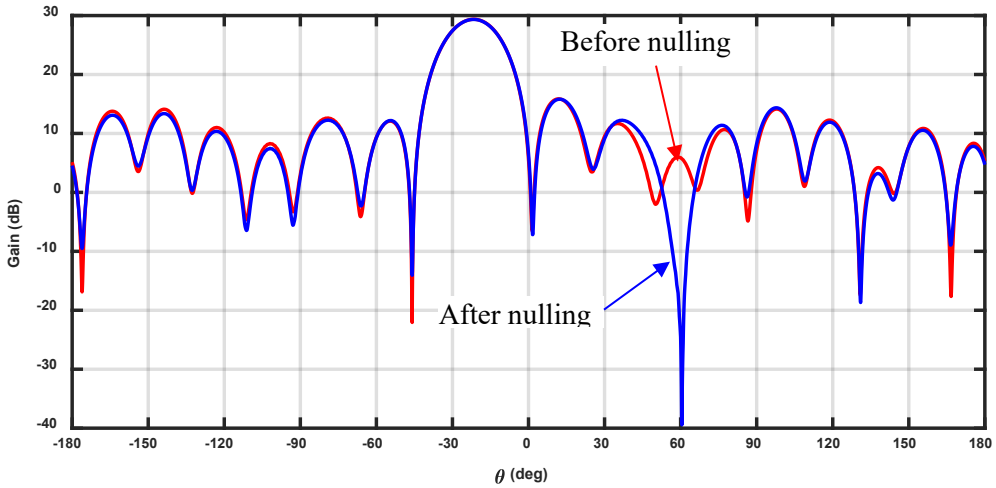

(a)

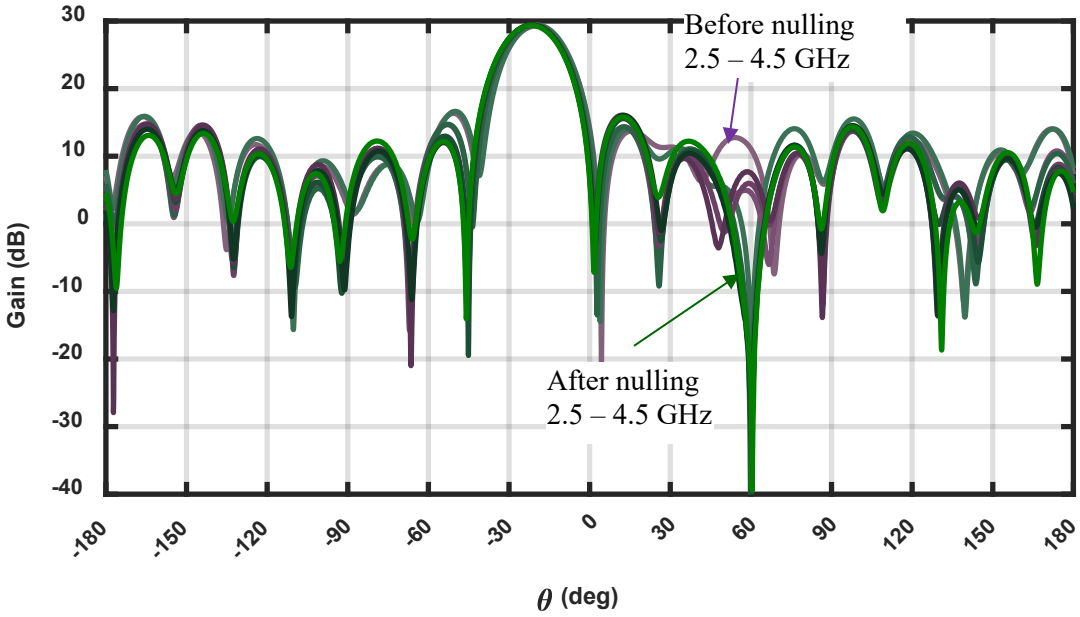

(b)

Figure 3-19: Beamforming from a 16-element circular array at (a) 4.5 GHz and (b) 2.5 GHz to 4.5 GHz at frequency resolution of 0.5 GHz.

4. CONCLUSION

As we reach the end of the 6.2 effort, we have completed and presented the following:

1. Developed designs of N-port Butler matrices.
2. Designed and optimized multiple wideband phase shifters that work from 2 GHz to 6 GHz.
3. Completed designs for 4 X 4 and 8 X 8 Butler matrices. These have been built, and we have measured and reported the results for the 4 X 4 Butler matrix.
4. Modeled, simulated and demonstrated beamforming via the use of a modal beamformer for an 8-element and 16-element circular array.
5. Demonstrated the formation of directional beams with a null for 8-element and 16-element beams.

In conclusion, we have shown that the use of a Butler matrix simplifies circular array beamforming such that only phase settings are needed to form directional beams. We have built 4 X 4 and 8 X 8 designs. Both have been measured and the measurements for the 4 X 4 presented in this report. The 8 X 8 design requires further processing and will be presented in future documentation.

5. REFERENCES

[1] R. Mital, M. P. Parent and A. Stumme, "Circular Array Beamforming using Phase Modes," NRL/ MR/5317-19-9908, Dec 16, 2019.

[2] H. Steyskal, "Digital beamforming aspects of wideband circular arrays," 2008 IEEE Aerospace Conference 2008, pp. 1-6.

[3] R. Mital, W. R. Pickles and M. P. Parent, "Design and Development of Butler Matrices for Circular Array Beamforming," NRL/MR/5317-20-10,130, September 22, 2020.

[4] J. L. Quirarte and J. P. Starski, "Synthesis of Schiffman Phase Shifters," *IEEE Transactions on Microwave Theory and Techniques,* vol. 39, no. 11, pp. 1885 - 1889, 1991.

[5] T. Macnamara, "Simplified design procedures for Bulter matrices incorporating 90deg hybrids or 180 deg hybrids," *IEE Proceedings,* vol. 134, no. 1, 1987.

[6] D. P. Scholnik, "Calibration and Optimization of a Wideband Circular Array Using a Phase-Mode Beamformer," NRL/5340/FR-2022/3, Dec 15, 2021.

[7] R. Mital and W. M. Dorsey, "Fast synthesis of multiple nulls in an omnidirectional pattern," in *IEEE International Symposium on Antennas and Propagation & USNC/URSI National Radio Science Meeting*, pp. 2011-2012 2017.